Supporting Information for

Electrodialysis and Nitrate Reduction (EDNR) to Enable Distributed Ammonia Manufacturing from Wastewaters

Jinyu Guo,[†] Matthew J. Liu,[†] Chloe Laguna,[†] Dean M. Miller,[†] Kindle Williams,[†] Brandon D. Clark,[†] Carolina Muñoz,[†] Sarah J. Blair,[†] Adam C. Nielander,[‡] Thomas F. Jaramillo,[†,‡] William A. Tarpeh[†,‡,*]

†Department of Chemical Engineering, Stanford University, Stanford, CA, 94305, USA

‡ SUNCAT Center for Interface Science and Catalysis, SLAC National Accelerator Laboratory, Menlo Park, CA, USA

56 pages
8 tables
40 figures
15 equations

*Corresponding author, Email: wtarpeh@stanford.edu. Address: 443 Via Ortega, Room 387, Stanford CA, 94305. Telephone: 650-497-1324

Table of Contents

Section S1. Experimental methods

Section S1.1 Chemicals

All chemical reagents were purchased from commercial vendors and used as received. Reagents used included titanium foil (Ti, 99.7%, 0.25 mm, Sigma-Aldrich), platinum foil (Pt, 99.99%, Sigma-Aldrich), IrO_2-Ta_2O_5/Ti mesh electrodes (Magneto Special Anodes, Schiedam), sodium perchlorate (≥ 98.0%, Sigma-Aldrich), sodium nitrate (≥ 99.0%, Sigma-Aldrich), nitric acid (67–70%, Fisher Chemical), potassium chloride (≥ 99.0%, Sigma-Aldrich), sodium sulfate (≥ 99.0%, Sigma-Aldrich), sodium chloride (≥ 99.0%, Fisher BioReagents), sodium phosphate dibasic (≥ 99%, Calbiochem), sodium citrate dihydrate (99.0−101.0%, Avantor Performance Materials), sodium nitroferricyanide dihydrate (Acros Organics), sodium hydroxide (≥ 97.0%, Ricca Chemical), sodium hypochlorite (10−15% available chlorine, Sigma-Aldrich), Dionex AS22 effluent concentrate (450 mM sodium carbonate, 140 mM sodium bicarbonate, Thermo Fisher), Dionex six cation-I standard (Thermo Fisher, 040187), Dionex seven anion standard (Thermo Fisher, 056933), phenol (≥ 99.0%, Sigma-Aldrich), isopropyl alcohol (99.5%, Acros Organics), L-(+)-tartaric acid (≥ 99.5%, Sigma-Aldrich), oxalic acid (98%, Sigma-Aldrich). Nanopure water (resistivity: 18.2 MΩ·cm, Millipore Sigma) was used for all experiments and measurements.

As-received platinum and titanium foil was cut into 5 cm × 2.5 cm pieces. All electrodes used in the experiment and cleaned through 5-minute ultrasonication (150 W ultrasonic power, 40 kHz frequency) in isopropyl alcohol followed by 5-minute ultrasonication in water, and dried using compressed air. A new piece of titanium foil was used for each EDNR experiment, while the platinum foil and IrO_2-Ta_2O_5/Ti mesh electrodes were cleaned as described above and reused.

Section S1.2 EDNR experiment procedures

All EDNR experiments took place in a polycarbonate, three-chamber compression cell with electrolyte flowing through each chamber from recirculation bottles, entering the cell through the bottom and exiting from the top (schematic shown in **Fig. S1**). Each recirculation bottle held 50 mL of respective electrolyte: NH_3 synthesis and NH_3 recovery chambers both held 0.1 M $KClO_4$ (in proof-concept) or 1 M $NaClO_4$ (in all other EDNR experiments), and the influent chamber held simulated or real wastewaters. The electrolyte flow rate was controlled by peristaltic pumps

(Masterflex model 07528-10 motor and model 77800-60 pump head, with 1/16-inch inner diameter tubing), and was constant for each experiment but differed between experiments (particularly those in which we probed the influence of flow rate on performance metrics). Note that an anion exchange membrane (AEM, two different types were used, as shown in Table 1 in the main manuscript) separated the NH_3 synthesis (left) and influent (middle) chambers, and a cation exchange membrane (CEM, CMI-7000, Membranes International) separated the influent (middle) and NH_3 recovery (right) chambers. Both AEM and CEM were immersed in 1 M $NaClO_4$ for over 24 hours before use to ensure proper hydration and expansion, and new pieces of membranes were used in each EDNR experiment. The cell consisted of one Ti electrode, two IrO_2-Ta_2O_5/Ti mesh electrodes, and one Pt electrode; these four electrodes were necessary to enable dynamic electrochemical bias switching between the electrodialysis (ED) stage and the nitrate reduction (NR) stage. In preparation for the experiment, the electrolyte was pumped through the cell for 15 minutes, after which the pumps were stopped, initial samples of 1 mL were taken from each recirculation bottle, and an initial potentiostatic electrochemical impedance spectroscopy (PEIS) at the open circuit voltage (OCV) was performed. Pumps were then turned back on.

A potentiostat (VSP, BioLogic for all experiments) was used to control the applied potential to the working electrode versus the leakless Ag/AgCl reference electrode (3.4 M KCl, ET072−1, eDAQ). All potentials were converted to the RHE scale with: $E_{Ag/AgCl} = E_{RHE} - 0.205\ V - 0.059 \times pH$. All electrochemical experiments were conducted using 85% IR compensation based on the ohmic resistance obtained via PEIS.

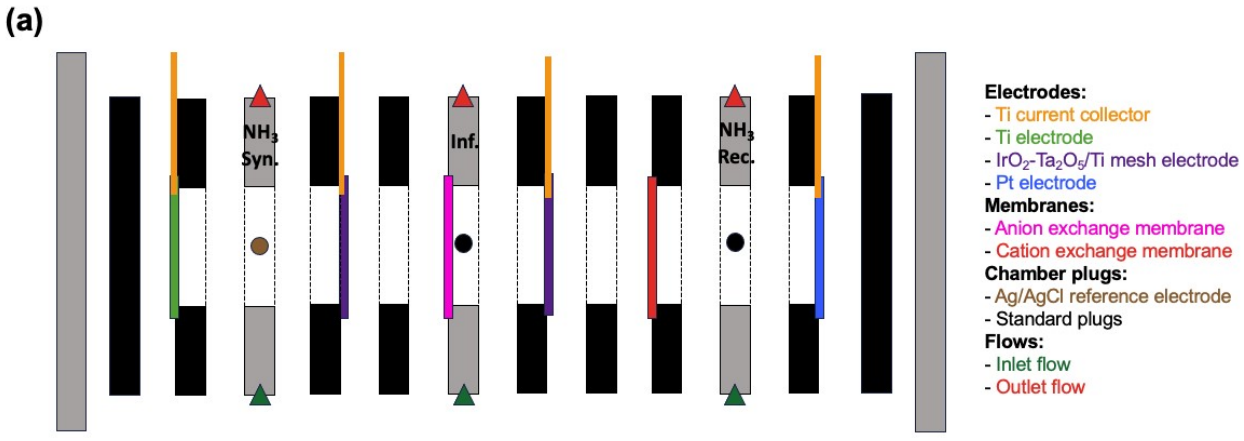

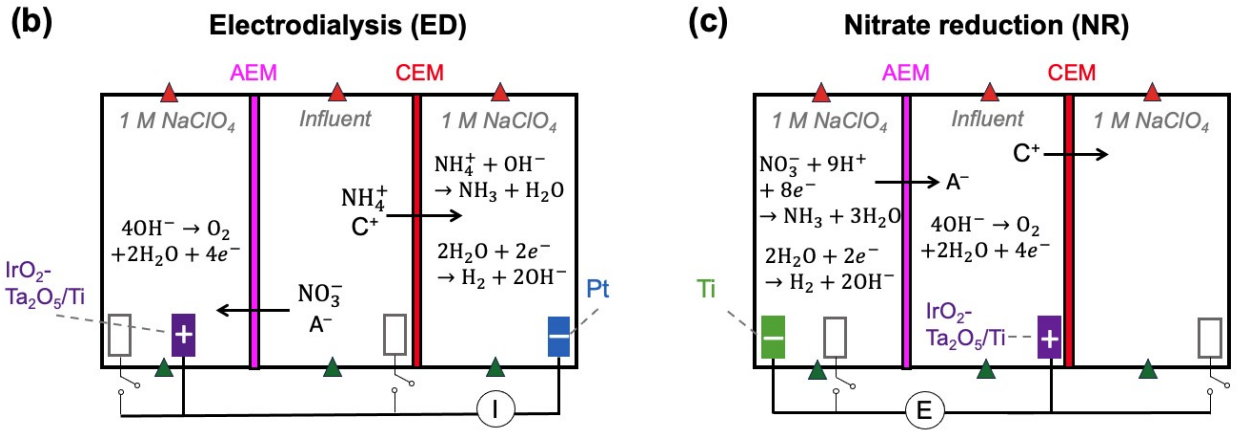

Figure S1. (a) Schematic of the EDNR reactor (side-view). Polycarbonate cell parts are shown in gray boxes; rubber gaskets are shown in black boxes, with dotted lines representing openings in the material. Triangles represent electrolyte ports, circles represent reference electrode or plugs, and colored squares represent electrodes or membranes, whose information is given by correspondingly colored legends. **(b)** Major electrode reactions and ion movement during the electrodialysis (ED) stage. C^+ represents cations, and A^- represents anions. **(c)** Major electrode reactions and ion movement during the nitrate reduction (NR) stage. Note that the electrolyte used in NH_3 synthesis and recovery chambers was 0.1 M $KClO_4$ in the proof-of-concept experiment and 1 M $NaClO_4$ in all other experiments, as shown in **(b)** and **(c)**. Additional experimental parameters are given in **Table S1**.

A. Electrodialysis (ED)

As the first stage of each cycle, electrodialysis (ED) was performed using IrO_2-Ta_2O_5/Ti mesh as the working electrode in the NH_3 synthesis chamber and Pt foil as the counter electrode in the NH_3 recovery chamber (**Fig. S2**). Note that no NH_3 synthesis is occurring during this stage, but the NH_3 synthesis chamber is named as such because it is the site of nitrate reduction to NH_3 in the second stage of each cycle. A constant current was applied for durations specified in **Table S1**. When necessary to avoid exceeding the full cell voltage limit, a lower current was applied over an extended ED duration to achieve the same charge passed. After experiment completion, the peristaltic pumps were stopped, and electrolyte samples of 1 mL were taken from each electrolyte reservoir in preparation for the second stage.

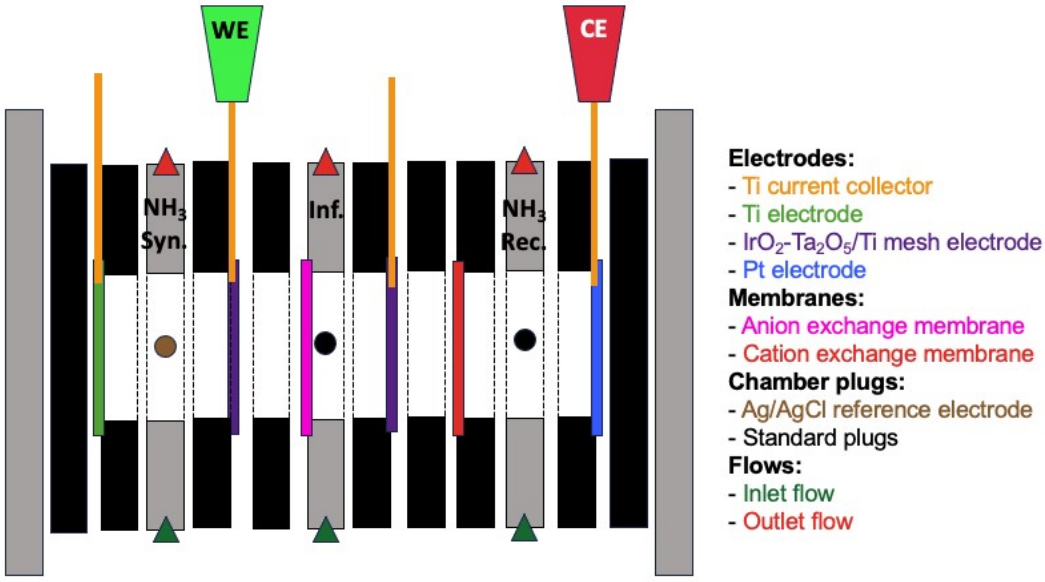

Figure S2. Schematic showing electrode connections to the potentiostat for electrodialysis (ED) stages. WE represents the working electrode, and CE represents the counter electrode. All other symbols follow the same convention as in **Fig. S1**: polycarbonate cell parts are shown in gray boxes; rubber gaskets are shown in black boxes, with dotted lines representing openings in the material. Triangles represent electrolyte ports, circles represent reference electrode or plugs, and colored squares represent electrodes or membranes, whose information is given by colored legends.

B. Nitrate reduction (NR)

Once electrodialysis was completed, nitrate reduction (NR) was performed as the second stage in every cycle. NR was performed using the Ti foil in the NH_3 synthesis chamber as the working electrode and the IrO_2-Ta_2O_5/Ti mesh in the influent chamber as the counter electrode (**Fig. S3**). PEIS was measured before peristaltic pumps were turned on. Nitrate reduction was then performed at –1.0 vs. RHE in a potentiostatic manner for 120 min (in proof-concept), or at –0.8 V vs. RHE in a pulsed potential manner (E_C = –0.8 V vs. RHE for t_C = 10 s, followed by E_A = OCV for t_A = 10 s) for a total duration of 120 min (in all other EDNR experiments).

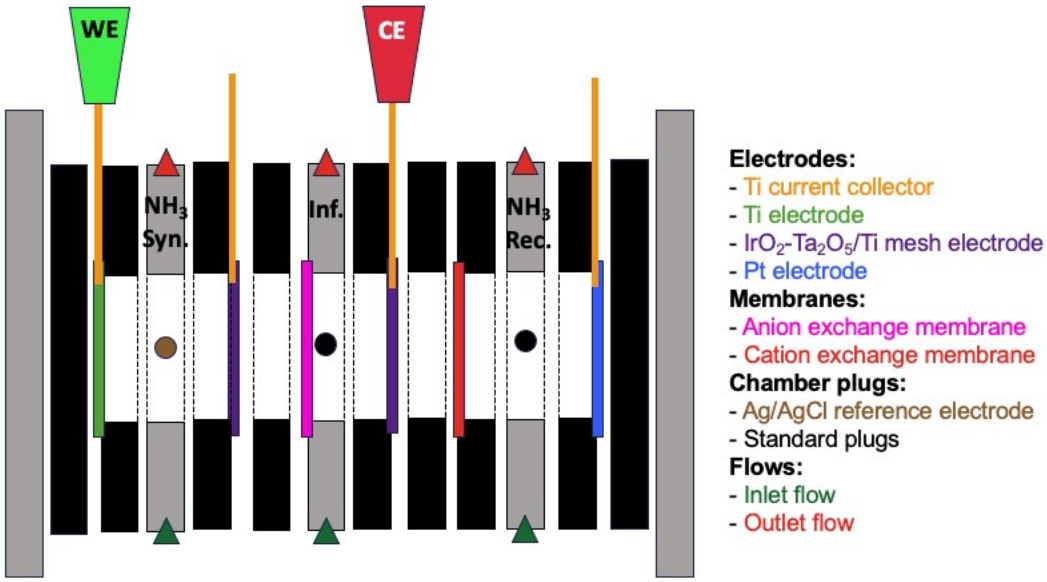

Figure S3. Schematic showing electrode connections to the potentiostat for nitrate reduction (NR) stages. WE represents the working electrode, and CE represents the counter electrode. All other symbols follow the same convention as in **Fig. S1**: polycarbonate cell parts are shown in gray boxes; rubber gaskets are shown in black boxes, with dotted lines representing openings in the material. Triangles represent electrolyte ports, circles represent reference electrode or plugs, and colored squares represent electrodes or membranes, whose information is given by colored legends.

Section S1.3 NR environment engineering experiment procedures

NR environment engineering experiments were performed in a polycarbonate, two-chamber compression cell divided by an anion exchange membrane (Selemion AMVN, same as in optimized NR), with a Ti working electrode, a Pt counter electrode chamber, and a Ag/AgCl reference electrode (**Fig. S4**). Each chamber held 10 mL of electrolyte, and the electrolytes were static during experiments (*i.e.*, no pumping, gas purging, or mechanical mixing).

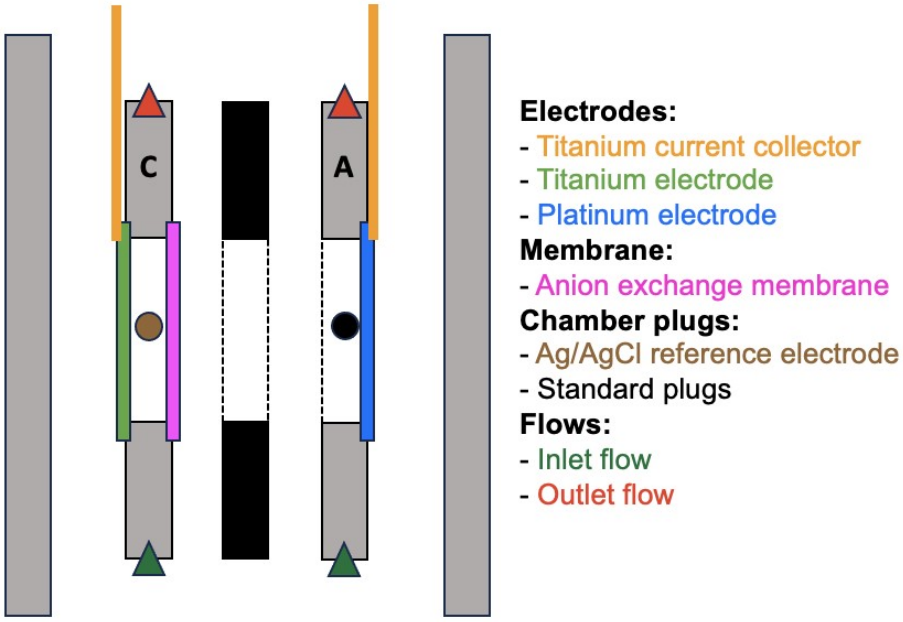

Figure S4. Schematic of electrolyte effects cell system. C represents the cathode, and A represents the anode. All other symbols follow the same convention as in **Fig. S1**: polycarbonate cell parts are shown in gray boxes; rubber gaskets are shown in black boxes, with dotted lines representing openings in the material. Triangles represent electrolyte ports, circles represent reference electrode or plugs, and colored squares represent electrodes or membranes, whose information is given by colored legends.

At the beginning of each experiment, 11 mL of electrolyte was added into the working and counter electrode chambers, respectively; 1 mL of electrolyte was taken from each chamber as the initial samples, leaving 10 mL in each chamber for the electrochemical experiment. PEIS was then conducted. Nitrate reduction was then performed at –0.8 V vs. RHE in a potentiostatic manner for 30 min. After the experiment, electrolytes were collected, and pH was adjusted as needed for product analysis (**Section S1.5**).

Section S1.4 Long-term EDNR experiment procedures

To test the long-term stability of the EDNR process, 4-cycle EDNR experiments were operated for five batches, treating 50 mL of fresh NH_4^+-enriched agricultural runoff influent in each batch. The operating parameters are given in **Table S1**. After the last NR stage in each batch (i.e., NR4), chronopotentiometry at –5.26 mA/cm^2 was applied to the Ti electrode for 15 min to basify the NH_3 synthesis chamber electrolyte and facilitate subsequent NH_3 extraction.

After each 4-cycle EDNR batch, we immediately pumped the NH_3-rich electrolytes from the NH_3 synthesis and recovery chambers in the EDNR reactor to the left and right feed chambers of a membrane stripping reactor, respectively. The middle chamber of the membrane stripping cell was a shared acid trap divided from the feed chambers with gas permeable membranes (Aquastill) on each side, and the acid trap was 20 mL of 42 mM H_3PO_4 (**Fig. S5**). In the membrane stripping reactor, volatile NH_3 in the feed chambers was extracted across two gas permeable membranes into H_3PO_4 solution in the acid trap chamber. All solutions were recirculated at 3.5 mL/min overnight, without any applied potential/current. After NH_3 extraction, 0.5 mL of liquid sample was drawn from the acid trap chamber, and the NH_3-depleted solutions in the feed chambers were directly reused as NH_3 synthesis and recovery chamber background electrolytes to minimize chemical input in the integrated unit process.

Before starting the next EDNR batch, 8 mL of fresh 1 M $NaClO_4$ was added to the NH_3 synthesis and to the recovery chambers to compensate for electrolyte volume loss due to sampling. The integrated 4-cycle EDNR (12-hr) + membrane stripping (overnight) unit process was conducted for five consecutive days, and a total of 250 mL NH_4^+-enriched agricultural runoff was processed.

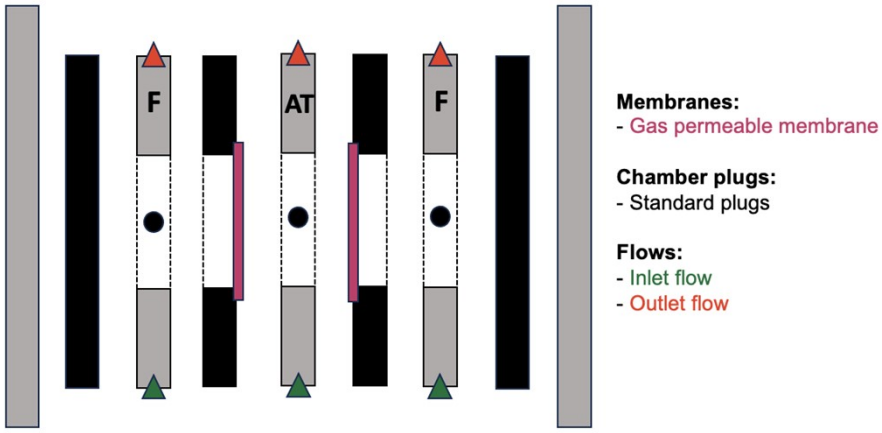

Figure S5. Schematic of membrane stripping cell. F represents feed, and AT represents acid trap. Inlet flows are shown in green, outlet flows are shown in red, and gas permeable membranes are shown in dark magenta. All other symbols follow the same convention as in **Fig. S1**: polycarbonate cell parts are shown in gray boxes; rubber gaskets are shown in black boxes, with dotted lines showing openings in the material. Triangles represent electrolyte ports and circles represent plugs.

Section S1.5 Sample analysis

Aqueous samples were analyzed using ion chromatography (ICS-6000, Dionex) and a flow injection analyzer (AA500 AutoAnalyzer, SEAL Analytical). To quantify Na^+, the sample aliquots were diluted 1000 times with nanopure water and analyzed using cation chromatography with 4 mM tartaric acid/2 mM oxalic acid eluent, SCS 1 column at 30 °C. The calibration range was 0.43–1.74 mM, and representative calibration data was shown in **Fig. S6a**. To quantify NO_3^-, NO_2^-, and ClO_4^- concentrations, the sample aliquots were basified with 5 wt% NaOH to pH > 10 (ensuring the complete dissociation of produced HNO_2 to the detectable NO_2^- anion form; pKa 3.16), diluted 30 times (for NO_3^- and NO_2^- quantification) or 500 times (for ClO_4^- quantification) with nanopure water and analyzed using anion chromatography with 4.5 mM CO_3^{2-}/0.8 mM HCO_3^- eluent and a AS23-4 μm column at 30 °C. The calibration range was 0.01–0.32 mM for NO_3^-, 0.01–0.44 mM for NO_2^-, and 0.5–10 mM for ClO_4^-; representative calibration data was shown in **Fig. S6b–d**. To quantify the concentration of NH_3, parallel sample aliquots were acidified with 2 M $HClO_4$ to pH < 2 (ensuring the complete protonation of produced NH_3 to the more stable NH_4^+ form; pKa 9.25) and analyzed using spectrophotometric flow injection analysis with the phenate method.[1] All bulk pH measurements were conducted using a pH meter (FiveEasy, Mettler Toledo). Note that all error bars shown in this manuscript represent ± one standard deviation from triplicate experiments, rather than triplicate sample analysis. Scanning electron microscopy (SEM) was performed using a Thermo Fisher Scientific Apreo S LoVac microscope, and energy dispersive X-ray spectroscopy (EDS) was carried out with a Bruker Quantax XFlash 6|60 EDS detector to analyze the elemental distribution on the electrodes and membrane surfaces. The membrane samples were mounted on aluminum pin stubs and sputter coated with gold to enhance the conductivity of the imaging surface. SEM images and EDS elemental maps were acquired at two locations on each sample.

Total organic and inorganic carbon (TOC and TIC) were measured using a Shimadzu TOC-L autoanalyzer (Shimadzu Scientific Instruments, Inc., Columbia, MD) at Environmental Measurements Facility at Stanford University.

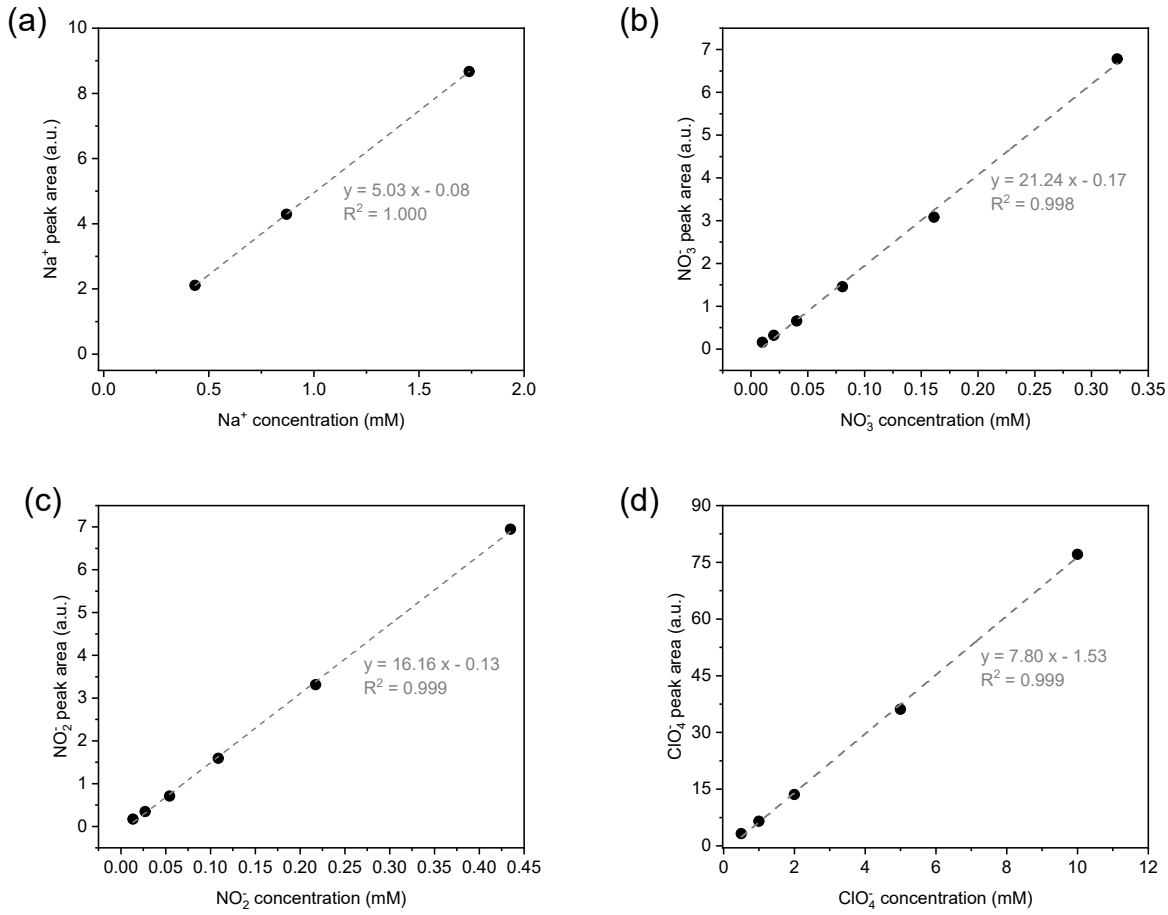

Figure S6. Ion chromatography calibration. **(a)** Na^+, **(b)** NO_3^-, **(c)** NO_2^-, and **(d)** ClO_4^-. Dotted lines show linear fitting of calibration data.

Section S1.6 Summary of reaction conditions

Table S1. Summary of electrolyte compositions and operating parameters used in EDNR experiments in this study.

Experiment sets	NH_3 Syn. Electrolyte	Influent	NH_3 Rec. Electrolyte	Electrolyte flow rate (mL/min)		ED1 j_{app} (mA/cm^2)	ED1 duration (min)	ED2 and ED3 j_{app} (mA/cm^2)	ED2 and ED3 duration (min)	NR E_{app} (V vs. RHE)*	NR duration (min)*
				ED	NR						
Proof-of-concept	0.1 M $KClO_4$	Simulated wastewater (13.9 mM $(NH_4)_2SO_4$ + 1.61 mM KNO_3)	0.1 M $KClO_4$	30	30	2.63	60	2.63	60	–0.6	120
Optimized NR	1 M $NaClO_4$		1 M $NaClO_4$	30	100	3.95	60	3.95	60	–0.8 (pulsed)	120#
Shortened ED				30	100	3.95	60	3.95	30		
Shortened ED + High flow				100	100	3.95	60	3.95	30		
NO_3^--laden		13.9 mM $(NH_4)_2SO_4$ + 26.4 mM KNO_3		30	100	3.95	60	3.95	60		
SO_4^{2-}-laden		13.9 mM $(NH_4)_2SO_4$ + 1.61 mM KNO_3 + 50 mM Na_2SO_4									
Cl^--laden		13.9 mM $(NH_4)_2SO_4$ + 1.61 mM KNO_3 + 100 mM NaCl									
RO retentate		RO retentate				3.95	60	3.95	60		
Well water		NH_4^+-enriched well water				3.95	60	3.95	45†		
Agricultural runoff		NH_4^+-enriched agricultural runoff				3.95	60	3.95	40†		
Agricultural runoff (4-cycle)		NH_4^+-enriched agricultural runoff		30	100	3.95	53.5†	3.95	50 (ED2)† 45 (ED3)† 40 (ED4)†		
Agricultural runoff (long-term)		NH_4^+-enriched agricultural runoff		100‡	100	3.95	60	2.93 (ED2) 2.16 (ED3) 2.12 (ED4)	60		

* Same applied potentials and durations were used in all NR stages.

For NR using pulsed potential, total NR duration is 120 min, and effective NR reaction time is 60 min.

† Durations of ED stages were shortened due to full cell voltage overload (20 V).

‡ A higher electrolyte flow rate was applied in ED stages to compensate for the decreased magnitude of applied current, which was intentionally lowered to avoid full cell voltage overload.

Section S1.7 Key performance metrics

For brevity, NH_3 synthesis, influent, and NH_3 recovery chambers are represented by Syn, Inf, and Rec, respectively in the equations below.

A. Electrodialysis (ED)

The following quantities were calculated to assess performance of the electrodialysis (ED) stage in EDNR.

NH_4^+ ED current efficiency (CE) in cycle *i*:

$$NH_4^+\ ED\ CE_{Cycle\ i}\,(\%) = \frac{(\left[NH_4^+\right]_{Inf,\ NR(i-1)} - \left[NH_4^+\right]_{Inf,\ EDi}) \times V_{Inf} \times F}{Q_{ED}} \times 100\% \qquad \textbf{Eqn. S1}$$

where $\left[NH_4^+\right]_{Inf,\ NR(i-1)}$ and $\left[NH_4^+\right]_{Inf,\ EDi}$ are the NH_4^+ concentrations in the influent chamber before and after ED in cycle *i* (mM), respectively, and $i-1=0$ represents the initial concentration before the EDNR experiment started; V_{Inf} is the total volume of the electrolyte in the influent chamber and its corresponding reservoir (50 mL); F is the Faraday constant (96485 C/mol); and Q_{ED} is the total charge passed during the ED stage (C).

NH_4^+ ED flux in cycle *i*:

$$NH_4^+\ ED\ flux_{Cycle\ i}\left(mmol \cdot cm^{-2} \cdot min^{-1}\right) = \frac{(\left[NH_4^+\right]_{Inf,\ NR(i-1)} - \left[NH_4^+\right]_{Inf,\ EDi}) \times V_{Inf}}{t_{ED} \times A_{ED}} \qquad \textbf{Eqn. S2}$$

where t_{ED} is the operation duration of the ED stage (min), and A_{ED} is the cross-sectional area of EDNR reactor chambers (5.7 cm^2).

Therefore,

$$NH_4^+\ ED\ flux_{Cycle\ i} = NH_4^+\ ED\ CE_{Cycle\ i} \times \frac{Q_{ED}}{t_{ED} \times A_{ED} \times F} \qquad \textbf{Eqn. S3}$$

Similarly, NO_3^- ED current efficiency in cycle *i*:

$$NO_3^-\ ED\ CE_{Cycle\ i}\,(\%) = \frac{(\left[NO_3^-\right]_{Inf,\ NR(i-1)} - \left[NO_3^-\right]_{Inf,\ EDi}) \times V_{Inf} \times F}{Q_{ED}} \times 100\% \qquad \textbf{Eqn. S4}$$

where $[NO_3^-]_{Inf,\ NR(i-1)}$ and $[NO_3^-]_{Inf,\ EDi}$ are the NO_3^- concentrations in the influent chamber before and after ED in cycle *i* (mM), respectively.

NO_3^- ED flux in cycle *i*:

$$NO_3^-\ ED\ flux_{Cycle\ i}\left(mmol \cdot cm^{-2} \cdot min^{-1}\right) = \frac{\left([NO_3^-]_{Inf,\ NR(i-1)} - [NO_3^-]_{Inf,\ EDi}\right) \times V_{Inf}}{t_{ED} \times A_{ED}} \quad \textbf{Eqn. S5}$$

And

$$NO_3^-\ ED\ flux_{Cycle\ i} = NO_3^-\ ED\ CE_{Cycle\ i} \times \frac{Q_{ED}}{t_{ED} \times A_{ED} \times F} \quad \textbf{Eqn. S6}$$

ED stage energy consumption in cycle *i*:

$$ED\ stage\ energy\ consumption_{\ Cycle\ i}\ (\text{MJ/kg } NH_3) = \frac{\int E_{cell} \times I\ dt}{\left([NH_3]_{Rec,\ EDi} - [NH_3]_{Rec,\ ED(i-1)}\right) \times V_{Rec} \times 17\frac{g}{mol} \times \frac{1\ kg}{1000\ g}} \quad \textbf{Eqn. S7}$$

where E_{cell} is the full cell voltage during ED stage in cycle *i* (V), I is the applied current in ED (A), and the electrical power ($E_{cell} \times I$) was integrated over the entire ED duration (J). $[NH_3]_{Rec,\ EDi}$ and $[NH_3]_{Rec,\ ED(i-1)}$ are the NH_3 concentrations in the NH_3 recovery chamber after ED in cycle $i-1$ and cycle *i* (mM), respectively. V_{Rec} is the total volume of the electrolyte in the NH_3 recovery chamber and its corresponding reservoir (50 mL).

B. Nitrate reduction (NR)

The following quantities were calculated to assess performance of the nitrate reduction (NR) stage in EDNR and in two-chamber NR environment engineering experiments.

Total current density:

$$j_{tot}(mA/cm^2) = \frac{Q_{NR}}{t_{NR} \times A_{NR}} \quad \textbf{Eqn. S8}$$

where Q_{NR} is the total charge passed during the NR stage ($mA \cdot s$), t_{NR} is the effective NR reaction time (the actual duration when a nitrate reduction potential was applied, s), and A_{NR} is the geometric area of the NR electrode (5.7 cm^2 in EDNR reactor and 5.4 cm^2 in two-chamber reactor).

NH_3 partial current density:

$$j_{NH_3}(mA/cm^2) = j_{tot} \times FE_{NH_3} \qquad \textbf{Eqn. S9}$$

where FE_{NH_3} is the Faradaic efficiency (%) of NH_3, see **Eqn. S11**.

Time-averaged NR NO_3^- removal rate:

NR NO_3^- removal rate ($\mu mol \cdot cm^{-2} \cdot min^{-1}$)

$$= \frac{([NO_3^-]_{Syn,\ NR(i-1)} - [NO_3^-]_{Syn,\ NRi}) \times V_{Syn}}{t_{NR} \times A_{NR}} \qquad \textbf{Eqn. S10}$$

where $[NO_3^-]_{Syn,\ NR(i-1)}$ and $[NO_3^-]_{Syn,\ NRi}$ are the NO_3^-concentrations in the NH_3 synthesis chamber after NR in cycle $i-1$ and cycle i (mM), respectively, and V_{Syn} is the total volume of the electrolyte in the NH_3 synthesis chamber and its corresponding reservoir (50 mL). For two-chamber experiments, $[NO_3^-]_{Syn,\ NR(i-1)}$ and $[NO_3^-]_{Syn,\ NRi}$ are the initial and final concentrations of NO_3^- in the cathode chamber (mM), respectively, and V_{Syn} is the total volume of the electrolyte in the cathode chamber (10 mL).

Faradaic efficiency (FE) of product j:

$$FE_j(\%) = \frac{nF([product\ j]_{Syn,\ NRi} - [product\ j]_{Syn,\ NR(i-1)})V_{Syn}}{Q_{NR}} \times 100\% \qquad \textbf{Eqn. S11}$$

where n is the stoichiometric number of electrons involved in the production of j ($n = 2$ for NO_2^-, 8 for NH_3), and $[\text{product } j]_{Syn,\ NRi}$ and $[\text{product } j]_{Syn,NR(i-1)}$ are the concentrations of j in the NH_3 synthesis chamber after NR in cycle $i-1$ and cycle i (mM), respectively, or final and initial concentrations in both cathode and anode chambers (mM) in two-chamber experiments. Note that NO_2^- could be lost into the influent chamber across the AEM and therefore undercounted in this calculation.

NR stage energy consumption in cycle *i*:

$$\text{NR stage energy consumption}_{Cycle\ i}\ (\text{MJ/kg NH}_3) = \frac{\int E_{cell} \times I\ dt}{\left([NH_3]_{Syn,\ NRi} - [NH_3]_{Syn,NR(i-1)}\right) \times V_{Syn} \times 17\frac{g}{mol} \times \frac{1\ kg}{1000\ g}} \quad \textbf{Eqn. S12}$$

where E_{cell} is the full cell voltage during NR stage in cycle *i* (V), I is the total current in NR (A), and the electrical power ($E_{cell} \times I$) was integrated over the entire NR duration (J), $[NH_3]_{Syn,\ NRi}$ and $[NH_3]_{Syn,\ NR(i-1)}$ are the NH_3 concentrations in the NH_3 synthesis chamber after NR in cycle $i-1$ and cycle *i* (mM), respectively.

Average energy consumption for NH_3 production in cycle *i*:

$$\text{Average energy consumption}_{for\ NH_3\ production\ Cycle\ i}\ (\text{MJ/kg NH}_3) = \frac{\left(\int E_{cell} \times I\ dt\right)_{EDi} + \left(\int E_{cell} \times I\ dt\right)_{NRi}}{\left[\left([NH_3]_{Rec,\ EDi} - [NH_3]_{Rec,\ ED(i-1)}\right) \times V_{Rec} + \left([NH_3]_{Syn,\ NRi} - [NH_3]_{Syn,NR(i-1)}\right) \times V_{Syn}\right] \times 17\frac{g}{mo}$$

Eqn. S13

Section S1.9 Nitrate concentrations used in typical fundamental research

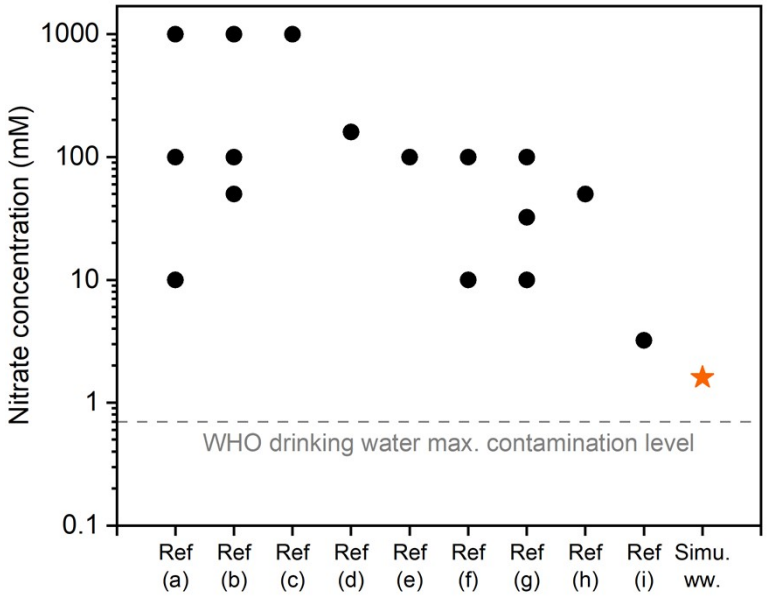

Figure S7. NO_3^- concentrations used in typical fundamental research. Dash line represents the maximum contamination level (MCL) for NO_3^- in drinking water set by the World Health Organization (10 ppm NO_3^--N).[2] Ref (a): McEnaney et. al.[3], Ref (b): Wu et. al.[4], Ref (c): Gao et. al.[5], Ref (d): Murphy et. al.[6], Ref (e): Crawford et. al.[7], Ref (f): Wang et. al.[8], Ref (g): Chen et. al.[9], Ref (h): Katsounaros et. al.[10], Ref (i): Wang et. al.[11]. Plot was adapted using data from our previous work[12] with authors' permission.

Section S2. Transference number calculations

We conducted back-of-the-envelope transference number calculations for influent chamber electrolyte in EDNR experiments to show the charge-carrying capabilities of different ions during ED using **Eqn. S14**.

$$t_j = \frac{i_j}{i} = \frac{|z_j| C_j \lambda_j}{\sum_k |z_k| C_k \lambda_k} \qquad \textbf{Eqn. S14}$$

where i_j is the current carried by ionic species j (mA), i is the total current (mA), z_j is the charge of ionic species j (unitless), C_j is concentration of ionic species j (mM), and λ_j is the ionic conductivity of ionic species j (S cm^2 mol^{-1}).

However, because the AEM and CEM were used between the influent and NH_3 synthesis chambers and the influent and NH_3 recovery chambers, respectively, we assumed complete blockage of counterions and calculated anion and cation transference numbers separately. It was assumed that ED current was carried solely by anion movement from NH_3 synthesis to influent chambers, and solely by cation movement from influent to NH_3 recovery chambers. All transference numbers calculated were based on the initial influent composition, and ionic conductivity data was from Zhong et al. [13]. Due to the near-neutral pH of all influents, H^+ and

OH^- are not included in transference number calculations due to their relatively low concentrations.

Table S2. Transference number calculations for simulated wastewater

Anion transference number (influent to NH_3 synthesis chambers)					
Ion	Charge	Concentration (mM)	Ionic conductivity (S cm^2 mol^{-1})	$\lvert z_j \rvert C_j \lambda_j$	Transference number
SO_4^{2-}	–2	13.9	160	4448	0.9750
NO_3^-	–1	1.6	71.42	114.272	0.0250
Total				4562.272	1

Cation transference number (influent to NH_3 recovery chambers)					
Ion	Charge	Concentration (mM)	Ionic conductivity (S cm^2 mol^{-1})	$\lvert z_j \rvert C_j \lambda_j$	Transference number
NH_4^+	+1	27.8	73.7	2048.86	0.9457
K^+	+1	1.6	73.5	117.6	0.0543
Total				2166.46	1

Note that the experimentally measured NH_4^+ ED current efficiency in ED1 is significantly lower than the calculated transference number, which we tentatively attribute to the CEM having a NH_4^+ to K^+ permselectivity ($P_{K^+}^{NH_4^+}$) lower than 1. In contrast, the experimentally measured NO_3^- ED current efficiency in ED1 is higher than the calculated transference number, possibly because the monovalent-selective AEM has a NO_3^- to SO_4^{2-} permselectivity ($P_{SO_4^{2-}}^{NO_3^-}$) higher than 1. While membrane development is beyond the scope of this EDNR study, future work could directly calculate the permselectivities for several ion combinations of the membranes used along with other possible membranes.

Table S3. Transference number calculations for NO_3^--laden simulated wastewater

Anion transference number (influent to NH_3 synthesis chambers)

Ion	Charge	Concentration (mM)	Ionic conductivity (S cm^2 mol^{-1})	$\lvert z_j \rvert C_j \lambda_j$	Transference number
SO^{2-}_4	–2	13.9	160	4448	0.6899
NO^-_3	–1	28	71.42	1999.76	0.3101
Total				6447.76	1.0000

Cation transference number (influent to NH_3 recovery chambers)					
Ion	Charge	Concentration (mM)	Ionic conductivity (S cm^2 mol^{-1})	$\lvert z_j \rvert C_j \lambda_j$	Transference number
NH^+_4	+1	27.8	73.7	2048.86	0.4989
K^+	+1	28	73.5	2058	0.5011
Total				4106.86	1.0000

Table S4. Transference number calculations for SO^{2-}_4-laden simulated wastewater

Anion transference number (influent to NH_3 synthesis chambers)					
Ion	Charge	Concentration (mM)	Ionic conductivity (S cm^2 mol^{-1})	$\lvert z_j \rvert C_j \lambda_j$	Transference number
SO^{2-}_4	–2	63.9	160	20448	0.9944
NO^-_3	–1	1.6	71.42	114.272	0.0056
Total				20562.272	1.0000

Cation transference number (influent to NH_3 recovery chambers)					
Ion	Charge	Concentration (mM)	Ionic conductivity (S cm^2 mol^{-1})	$\lvert z_j \rvert C_j \lambda_j$	Transference number
NH^+_4	+1	27.8	73.7	2048.86	0.2855
K^+	+1	1.6	73.5	117.6	0.0164
Na^+	+1	100	50.11	5011	0.6982
Total				7177.46	1.0000

Table S5. Transference number calculations for Cl^--laden simulated wastewater

Anion transference number (influent to NH_3 synthesis chambers)

Ion	Charge	Concentration (mM)	Ionic conductivity (S cm^2 mol^{-1})	$\lvert z_j \rvert C_j \lambda_j$	Transference number
SO^{2-}_4	–2	13.9	160	4448	0.3648
NO^-_3	–1	1.6	71.42	114.272	0.0094
Cl^-	–1	100	76.31	7631	0.6258
Total				12193.272	1.0000

Cation transference number (influent to NH_3 recovery chambers)					
Ion	Charge	Concentration (mM)	Ionic conductivity (S cm^2 mol^{-1})	$\lvert z_j \rvert C_j \lambda_j$	Transference number
NH^+_4	+1	27.8	73.7	2048.86	0.2855
K^+	+1	1.6	73.5	117.6	0.0164
Na^+	+1	100	50.11	5011	0.6982
Total				7177.46	1.0000

Section S3. Supplementary results

Section S3.1 Proof-of-concept EDNR

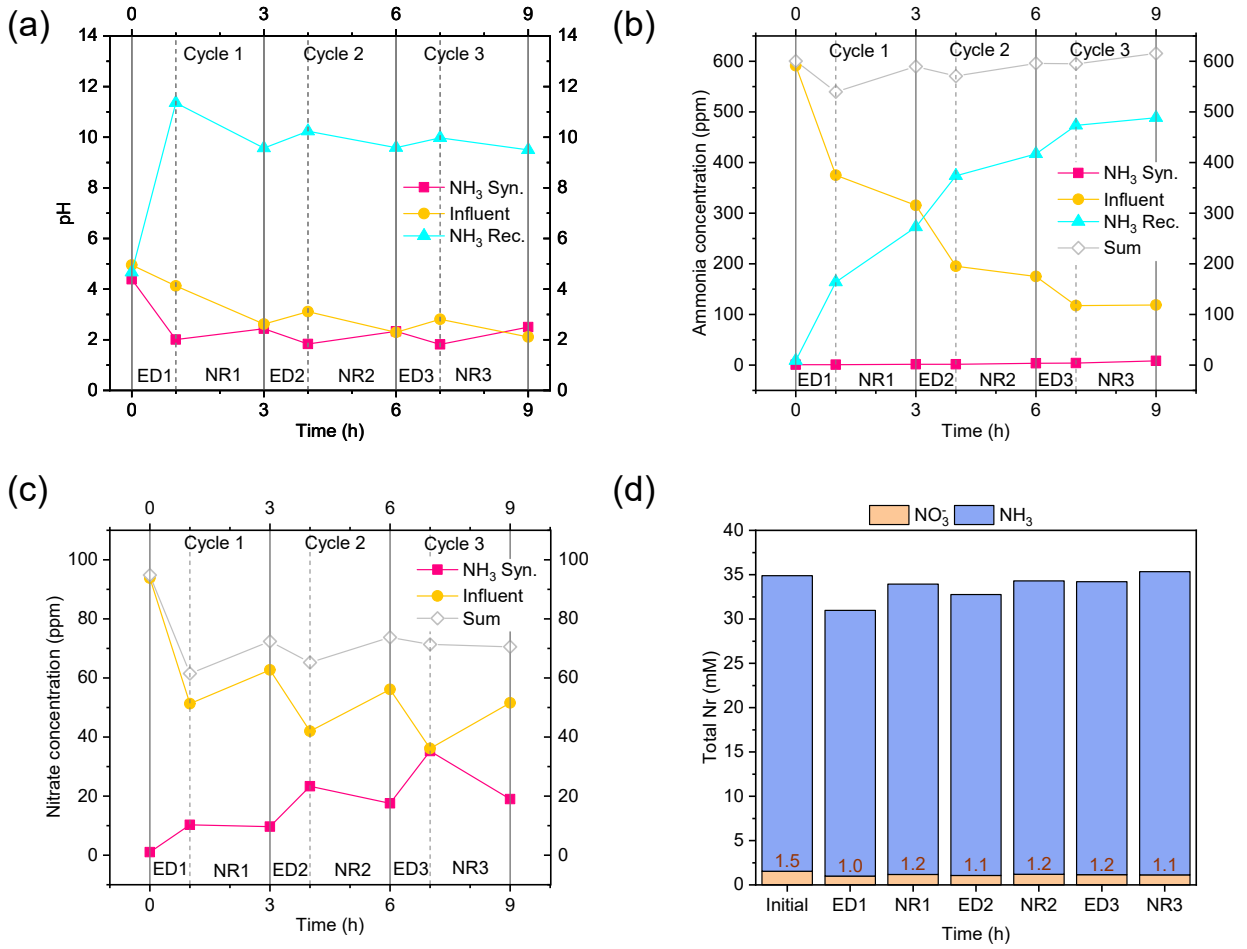

Figure S8. Proof-of-concept experiment. (a) pH trend, **(b)** NH_3 concentration trend and **(c)** NO_3^- concentration trend. EDNR cycles are indicated by solid vertical lines and stages are indicated by dashed vertical lines. Sum in (b) is the sum of NH_3 concentrations in all three chambers, and sum in (c) is the sum of NO_3^- concentrations in NH_3 synthesis and influent chambers. **(d)** Total Nr balance in the ENDR system (i.e., all three chambers and their corresponding electrolyte reservoirs).

Section S3.2 Engineering of EDNR operating parameters

Section S3.2.1 Reaction environment effects on nitrate reduction reaction

To amplify effects of NO_3RR electrolyte compositions, we fixed the NO_3^- concentration at 10 mM, slightly higher than typical EDNR influent levels. An applied potential of –0.8 V vs. RHE was found to balance NR activity and NR selectivity on Ti under similar NO_3^- concentrations in previous reports,[12] and thus was used in all subsequent experiments.

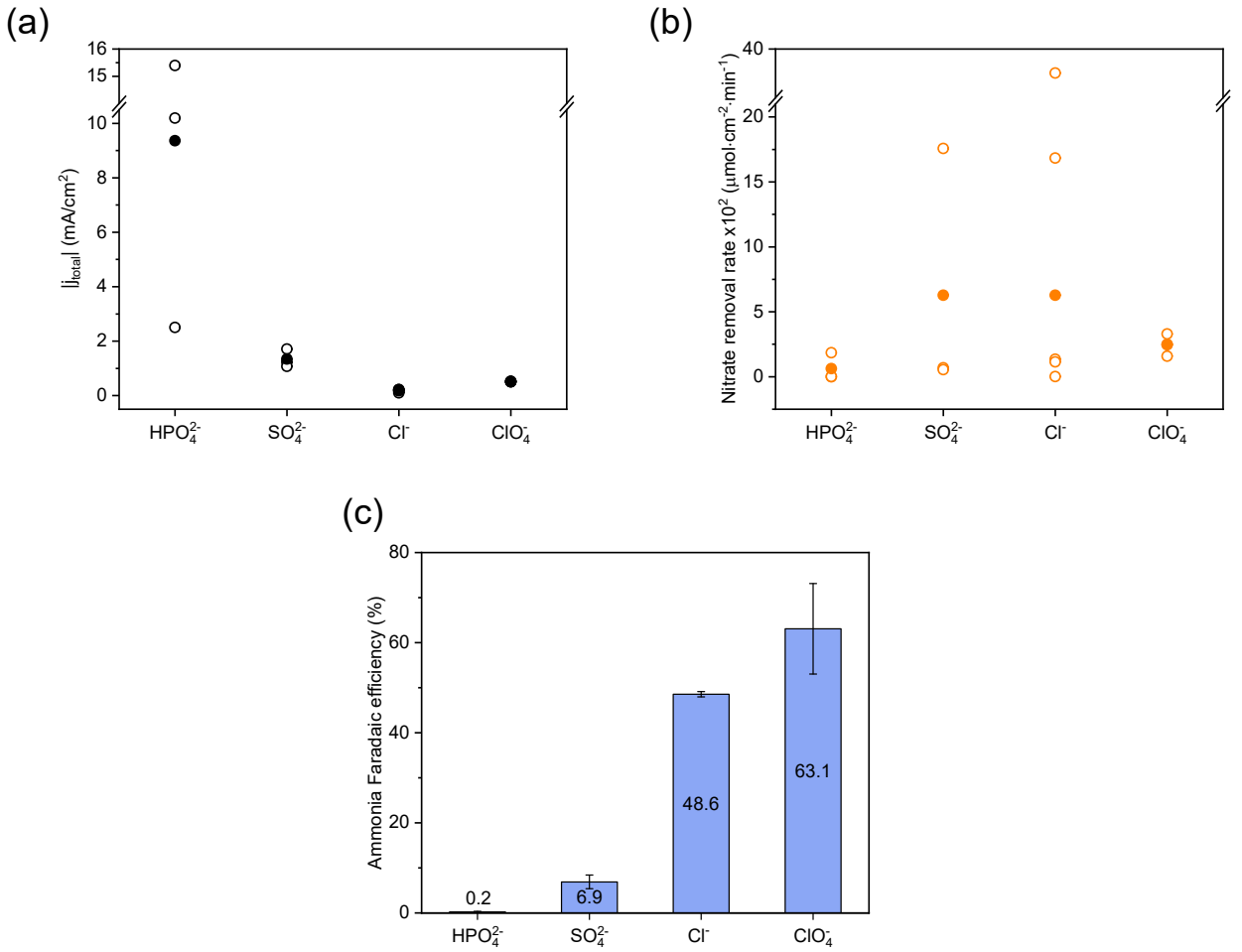

Figure S9. Anion effects on nitrate reduction reaction. (a) Total current density. **(b)** Time-averaged NO_3^- removal rate. Unfilled symbols in (a) and (b) represent results from individual replicate experiments, and filled symbols represent the average value in this background electrolyte. **(c)** NH_3 Faradaic efficiency from two-chamber experiments. Error bars represent ± one standard deviation. Background electrolytes: 10 mL 0.5 M Na_2HPO_4, or 0.5 M Na_2SO_4, or 1 M NaCl or 1 M $NaClO_4$, pH adjusted to 1.72 with 2 M $HClO_4$,

and 10 mM $NaNO_3$ was added to the cathode chamber. Applied potential: –0.8 V vs. RHE. Reaction duration: 30 min.

While a very high total current density was observed in the HPO_4^{2-} background (**Fig. S9a**), HER likely dominated, and only minimal NO_3^- was reduced (**Fig. S9b**). This dominant HER likely originated from facile proton donation from phosphate species, consistent with previous reports.[14–16] SO_4^{2-} and Cl^- backgrounds exhibited high-variance NO_3RR activity, possibly due to competitive adsorption on a variety of facets of the polycrystalline Ti electrode.[17] The most weakly adsorbing ClO_4^- background generated moderate but lower-variance total current density and NO_3^- removal rate. FE_{NH_3} was highest in the ClO_4^- background (63.1±10.1%), suppressed slightly in Cl^- (48.6±0.6%), and almost negligible in SO_4^{2-} and HPO_4^{2-} (<7%) (**Fig. S9c**). We have shown in a previous study that hydrogen evolution reaction (HER) and Ti hydride formation compete with electrochemical nitrate reduction on Ti foil.[18] Within nitrate reduction, NH_3 and NO_2^- account for >72% nitrogen products under similar reaction conditions (–0.8 V vs. RHE, 10 mM NO_3^-, pH 1.7).[12] Thus, the remaining FE most likely went into HER and Ti hydride formation.

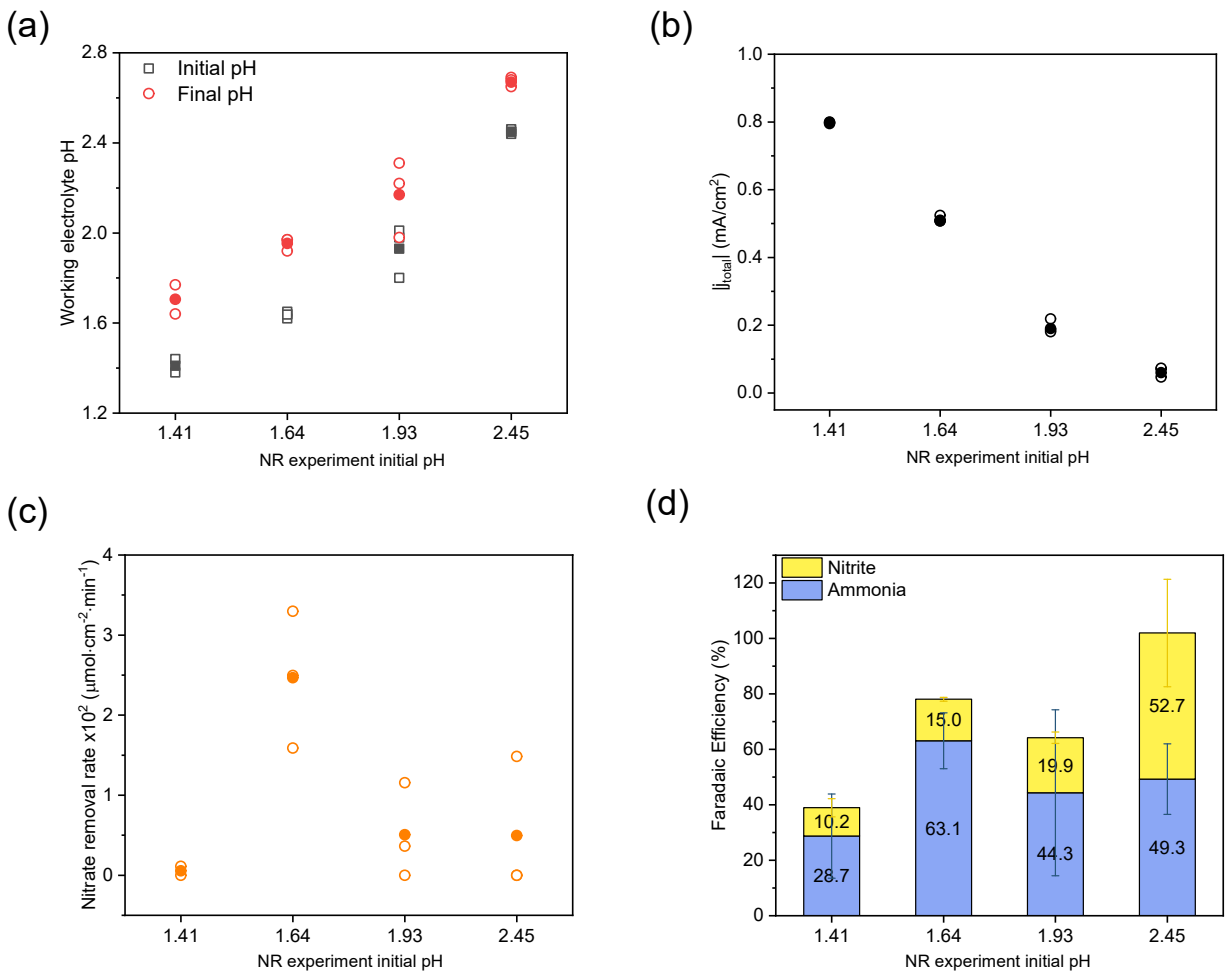

Figure S10. pH effects on nitrate reduction reaction. (a) Initial and final pH in the working electrode chamber. **(b)** Total current density. **(c)** Time-averaged NO_3^- removal rate. Unfilled symbols in (a)–(c) represent results from individual replicate experiments, and filled symbols represent the average value. **(d)** Faradaic efficiency from two-chamber experiments. Error bars represent ± one standard deviation. The higher than unity sum FE of NH_3 and nitrite in pH 2.45 reflects accumulated product analysis errors that originated from the very low total charge passed in NR. Electrolytes: 10 mL 1 M $NaClO_4$, pH adjusted to 1.41, 1.64, 1.93, and 2.45 with 2 M $HClO_4$, and 10 mM $NaNO_3$ was added to the cathode chamber. Applied potential: –0.8 V vs. RHE. Reaction duration: 30 min.

Within the pH range explored, the working electrode chamber pH generally increased by <0.2 units after reaction (**Fig. S10a**). The total current density decreased monotonically with increasing initial pH (**Fig. S10b**), but the highest NO_3^- removal rate was observed at pH 1.64 (**Fig. S10c**). Below pH 1.64, significantly lower nitrate reduction FE (<40%) was attributed to severe

HER and/or Ti hydride formation; above pH 1.64, $^{FE_{NH_3}}$ was impaired while $^{FE_{NO_2^-}}$ was enhanced (**Fig. S10d**).

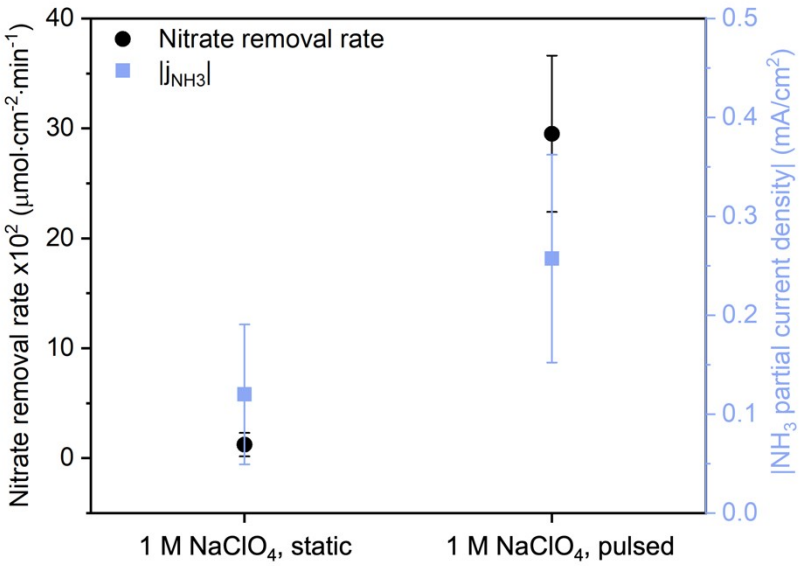

Figure S11. Applied potential profile effects on nitrate reduction reaction. Comparison of time-averaged $^{NO_3^-}$ removal rate (black circles, left axis) and NH_3 partial current density (purple squares, right y-axis) in static and pulsed potential experiments. Electrolyte for both chambers: 10 mL 1 M $NaClO_4$ + 10 mM HNO_3. Static potential: –1.0 V vs. RHE, 30 min. Pulsed potential: E_{WE} = –1.0 V vs. RHE for 10 s, followed by E_{WE} = OCV – 300 mV for 10 s, total reaction duration of 60 min (i.e., effective reduction time of 30 min). Error bars represent ± one standard deviation.

Section S3.2.2 Implementation of NR environment engineering to EDNR

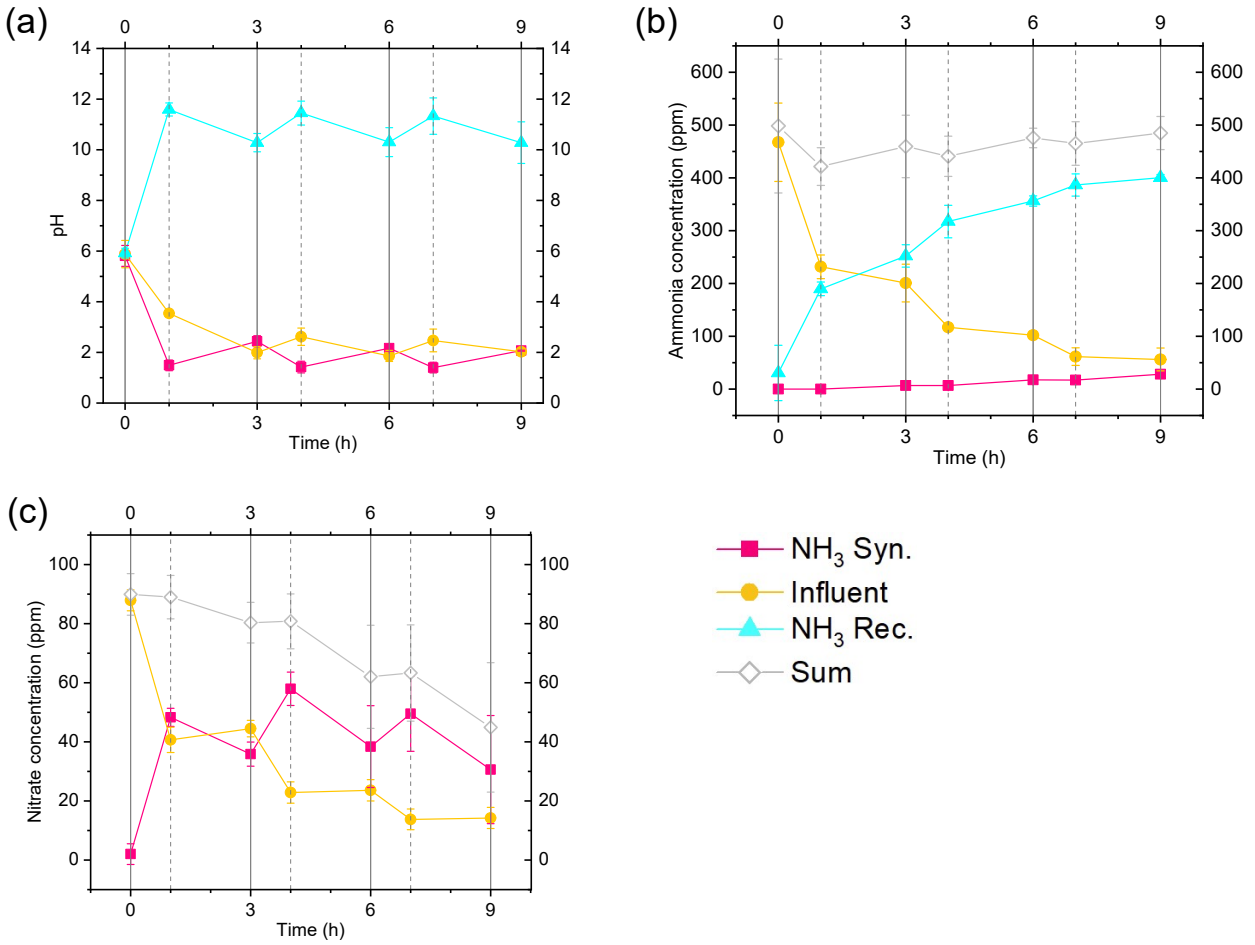

Figure S12. Optimized NR experiment trends. (a) pH trend, **(b)** NH_3 concentration trend and **(c)** $^{NO_3^-}$ concentration trend. EDNR cycles are indicated by solid vertical lines and stages are indicated by dash vertical lines. Same legends apply to all figures. Sum in (b) is the sum of NH_3 concentrations in all three chambers, and sum in (c) is the sum of $^{NO_3^-}$ concentrations in NH_3 synthesis and influent chambers. Error bars represent ± one standard deviation.

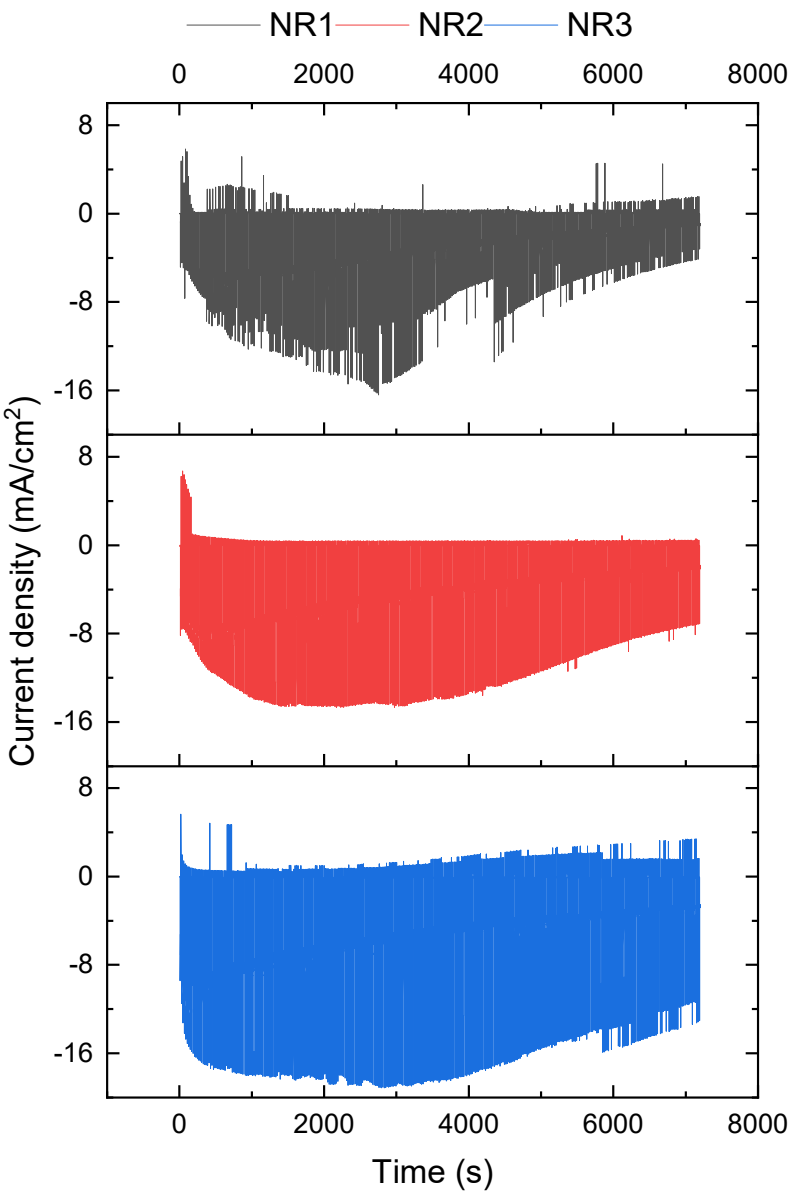

Figure S13. NR stage chronoamperometry from a representative optimized NR experiment.

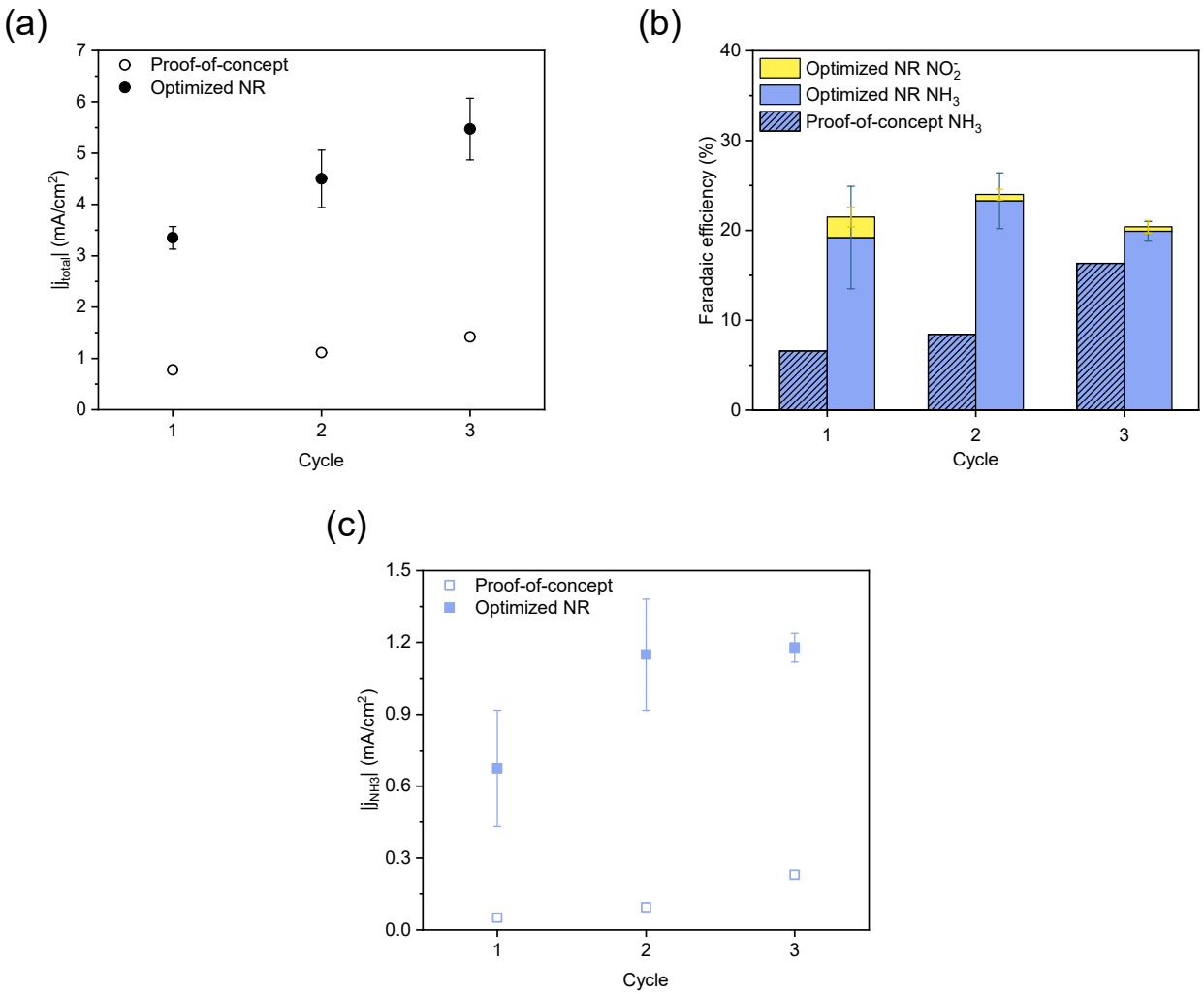

Figure S14. Optimized NR experiment NR performance. Comparison of **(a)** absolute value of total current density, **(b)** Faradaic efficiency and **(c)** absolute value of NH_3 partial current density in NR stages in proof-of-concept and optimized NR experiments. Error bars represent ± one standard deviation for triplicate optimized NR experiments (proof of concept n=1). The total current density during NR increased with cycle number, likely due to increased surface roughness over time.

NH_4^+ and NO_3^- ED fluxes were proportional to their current efficiency (**Eqn. S3** and **Eqn. S6**) and showed the same trend with respect to cycle number, which aligns with the decreasing trends of influent chamber NH_4^+ and NO_3^- concentrations (**Fig. S12, Fig. S15–16**). Because the amount of NH_4^+ and NO_3^- migrated during ED were a few times below the ion exchange capacities of the CEM[19] and AEM[20], respectively, and the applied current was three orders of magnitude lower than the theoretical limiting current predicted by the Rosenberg-Tirrell equation,[21] transport

from influent to the CEM/AEM (rather than transport across the CEM/AEM) likely controlled Nr removal from the influent.

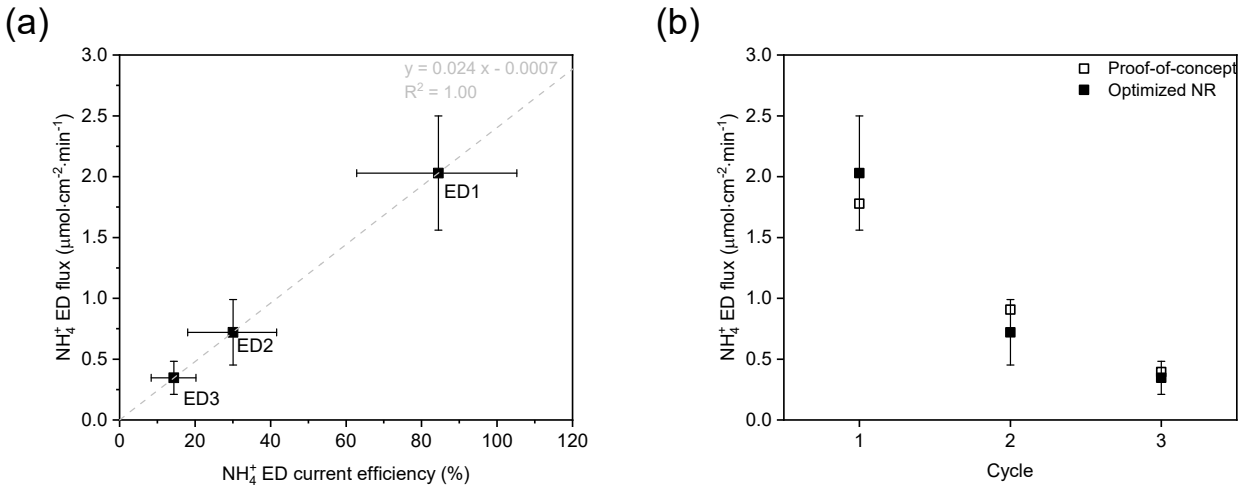

Figure S15. Optimized NR experiment ED performance for NH_4^+. (a) Relation between NH_4^+ ED flux and NH_4^+ ED current efficiency, as predicted by **Eqn. S3**. **(b)** NH_4^+ ED flux as a function of cycle number, in comparison with proof-of-concept experiments. Error bars represent ± one standard deviation for triplicate optimized NR experiments (proof of concept n=1).

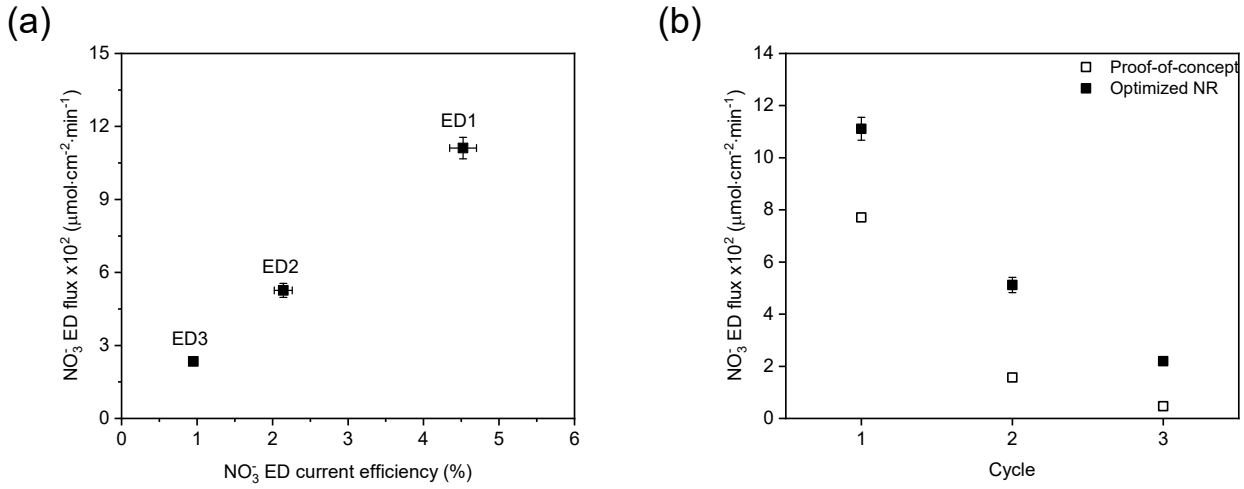

Figure S16. Optimized NR experiment ED performance for NO_3^-. (a) Relation between NO_3^- ED flux and NO_3^- ED current efficiency, as predicted by **Eqn. S6**. **(b)** NO_3^- ED flux as a function of cycle number, in comparison with proof-of-concept experiments. Error bars represent ± one standard deviation for triplicate optimized NR experiments (proof of concept n=1).

Section S3.2.3 Influence of ED stage operating parameters

First, we found that reducing the ED duration inhibited NH_3 recovery and NO_3^- removal from the influent. By halving the durations in ED2 and ED3 (referred to as short ED experiments), NH_4^+ ED current efficiency was not statistically different from optimized NR (**Fig. S18a**), but the end-of-run η_{Recovery} dropped from 0.84 ± 0.10 to 0.66 ± 0.02 due to reduced total ED charge (**Fig. S18c**). NO_3^- ED current efficiency was only slightly improved in short ED, but the end-of-run influent NO_3^- removal decreased slightly from $84 \pm 4\%$ to $73 \pm 7\%$ (**Fig. S18b**). Despite having similar NO_3^- concentrations at the beginning of NR stages with optimized NR (**Fig. S19a**), short ED exhibited dramatically lower $\eta_{\text{Synthesis}}$, which dropped from 1.11 ± 0.12 to 0.36 ± 0.28 at the end of the run (**Fig. S19f**). We attributed this inferior NR performance to higher initial bulk pH in the NH_3 synthesis chamber (~0.5 units higher than in optimized NR, **Fig. S19b**). The insufficient acidity led to substantially lowered NR activity and FE_{NH_3} (approximately half of values in optimized NR, **Fig. S19c-e**), highlighting the sensitivity of NR performance to the electrolyte pH.

We kept the short ED durations but enhanced mass transport in ED by increasing the electrolyte flow rate from 30 to 100 mL/min (in all chambers), the same as the flow rate used in NR stages (referred to as short ED + high flow rate experiments). However, ED current efficiencies for NH_4^+ and NO_3^- were not appreciably improved, and influent NO_3^- removal remained similar to Short ED. The largely unaltered Nr removal indicates that the Nr transport from the influent chamber to the AEM/CEM might be controlled by electromigration rather than diffusion and convection under this condition. In contrast, η_{Recovery} was enhanced by 25%–35% in all cycles relative to short ED, restoring the values observed in the optimized NR case (**Fig. S18c**). The enhanced NH_3 recovery suggested NH_3 transport from the CEM to the NH_3 recovery chamber was also sluggish under this condition and was facilitated by the enhanced mass transport. Compared to short ED, similar NH_3 synthesis chamber pH and NO_3^- concentrations were achieved at the beginning of each NR stage (**Fig. S19a–b**), and $\eta_{\text{Synthesis}}$ was not statistically improved as a result (**Fig. S19f**).

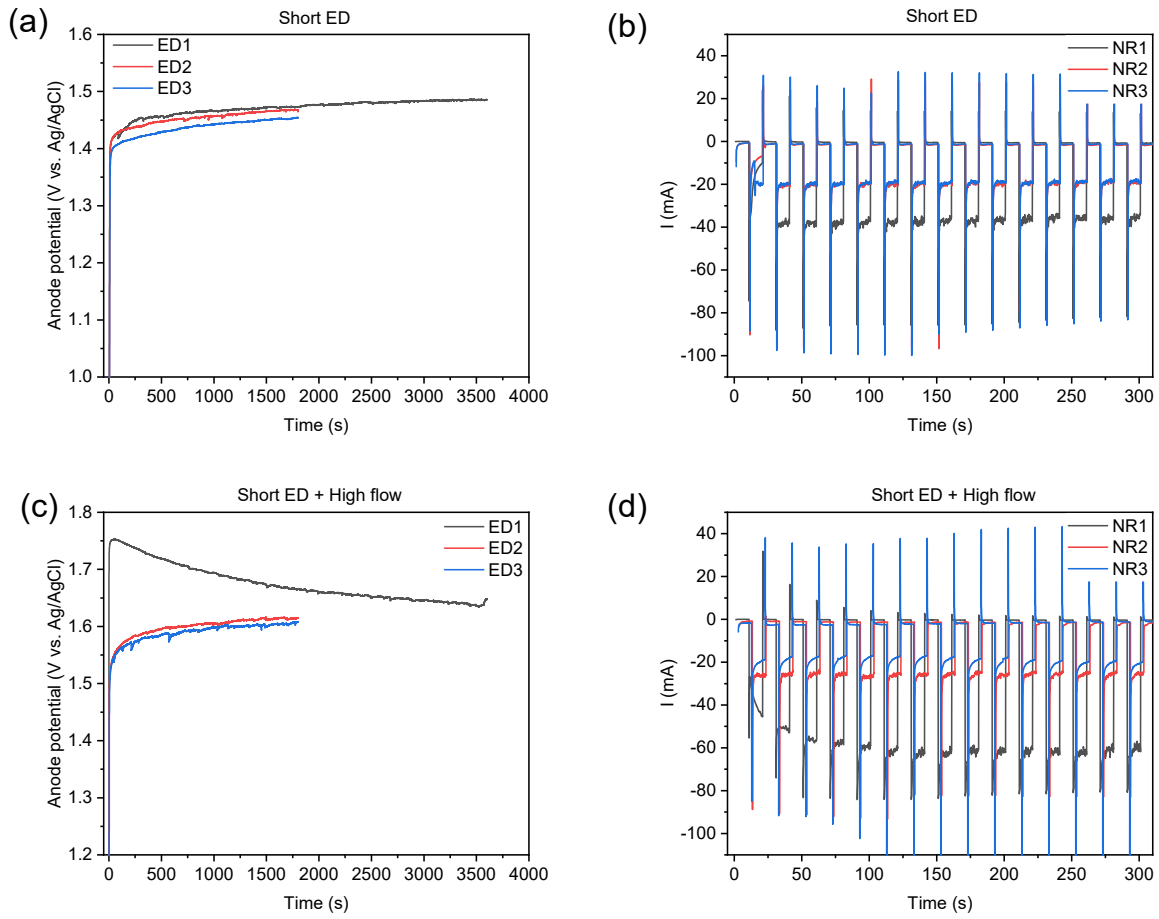

Figure S17. Chronopotentiometry and chronoamperometry data from ED operating parameters study. (a) Anode (IrO_2-Ta_2O_5/Ti mesh electrode in the NH_3 synthesis chamber) potentials as functions of time in ED stages and **(b)** cathode (Ti electrode in the NH_3 synthesis chamber) current in the first 5 min into each NR stage in the short ED experiments. **(c)** Anode (IrO_2-Ta_2O_5/Ti mesh electrode in the NH_3 synthesis chamber) potentials as functions of time in ED stages and **(d)** cathode (Ti electrode in the NH_3 synthesis chamber) current in the first 5 min into each NR stage in the short ED + high flow experiments. The average total current density from NR stages in both sets of experiments are given in **Fig. S19c**.

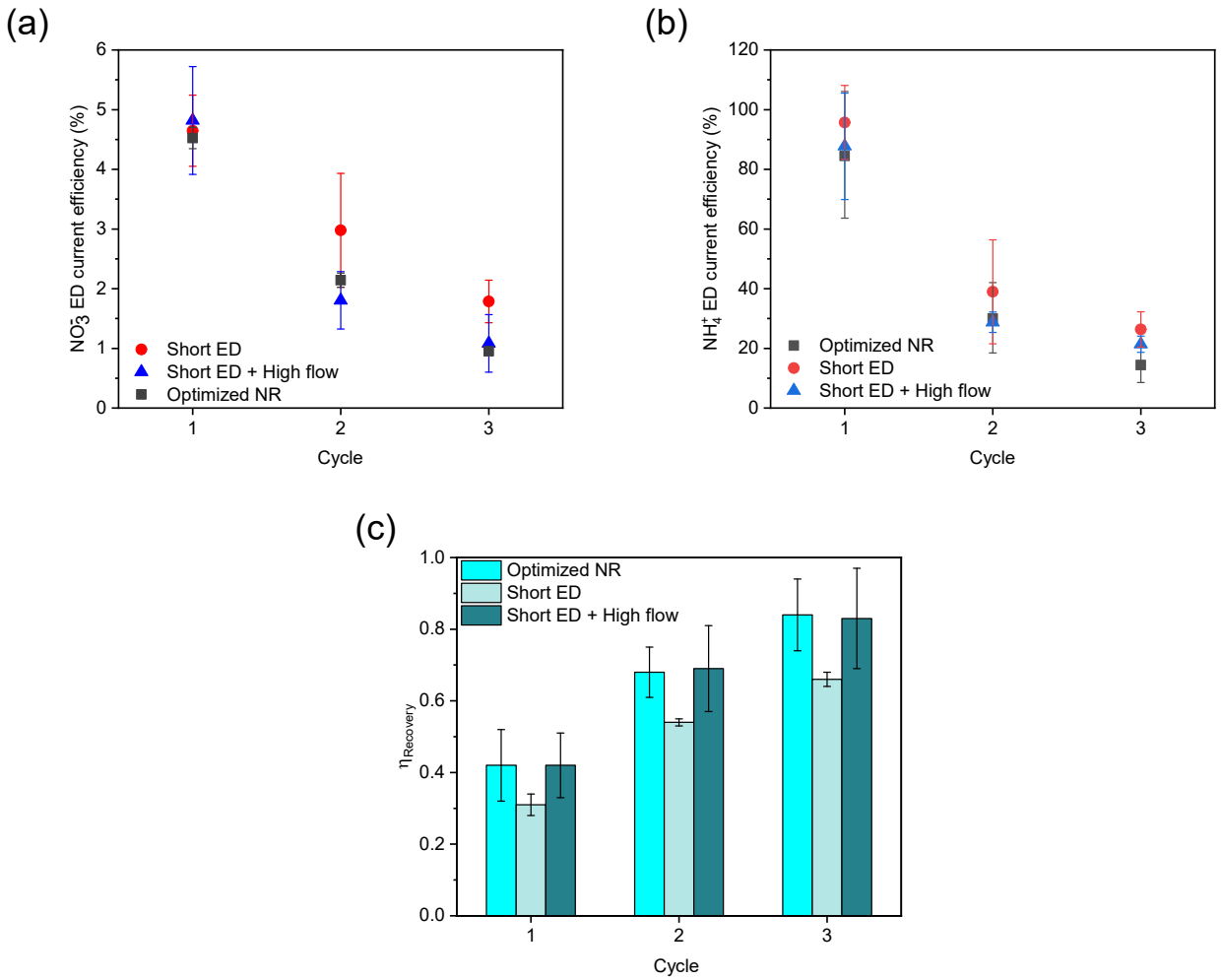

Figure S18. ED operating parameters effects on ED. (a) NH_4^+, **(b)** NO_3^- ED current efficiencies and **(c)** NH_3 recovery efficiency, in comparison with optimized NR experiments. Error bars represent ± one standard deviation.

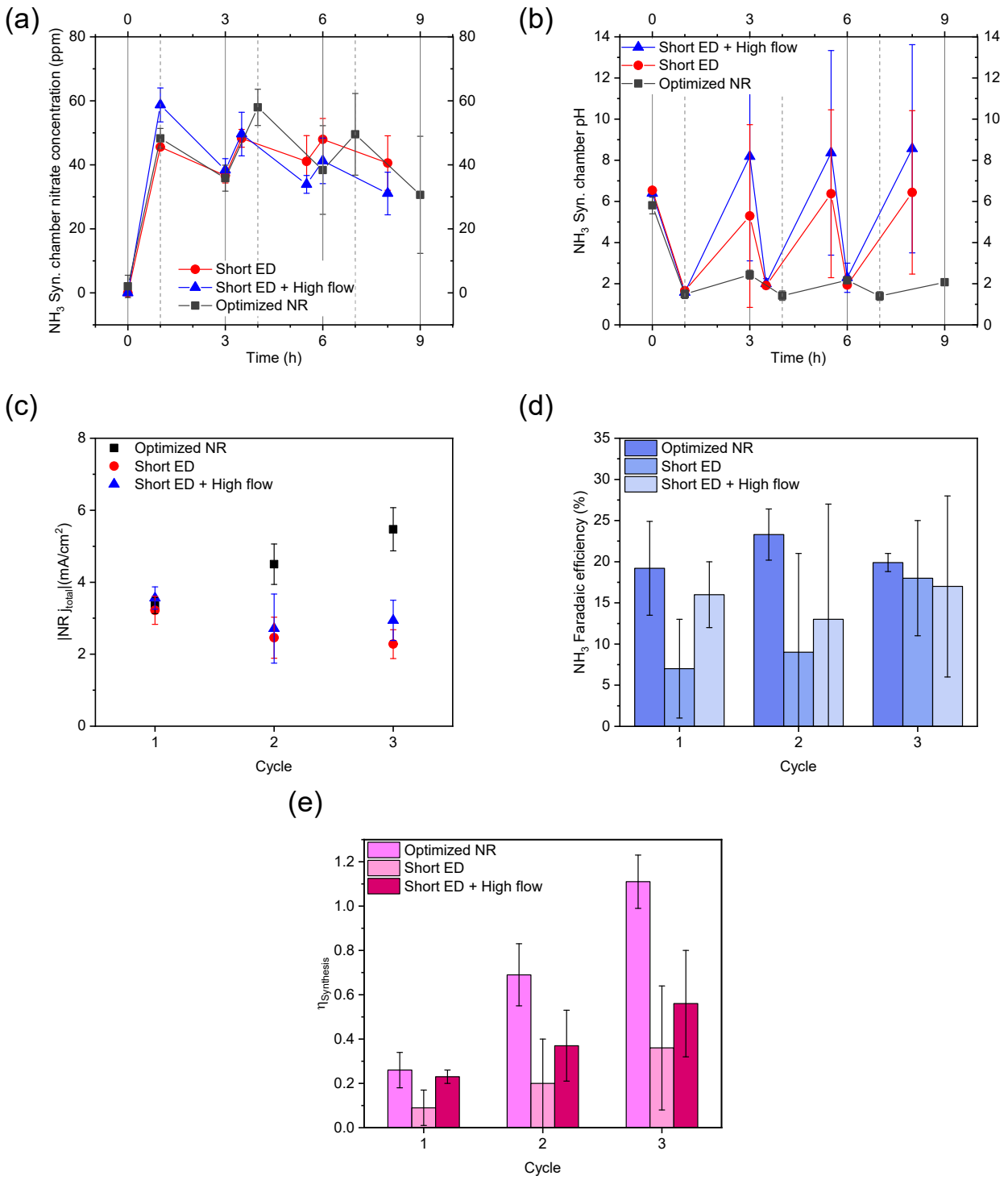

Figure S19. ED operating parameters effects on NR. (a) NH_3 synthesis chamber pH trend and **(b)** NH_3 synthesis chamber NO_3^- concentration trend, **(c)** absolute value of total current density and **(d)** NH_3 Faradaic efficiency in NR stages, and **(e)** NH_3 synthesis efficiency compared to optimized NR experiments. Error bars represent ± one standard deviation.

Section S3.3 Impacts of influent compositions on EDNR performance

Section S3.3.1 Modified simulated wastewater

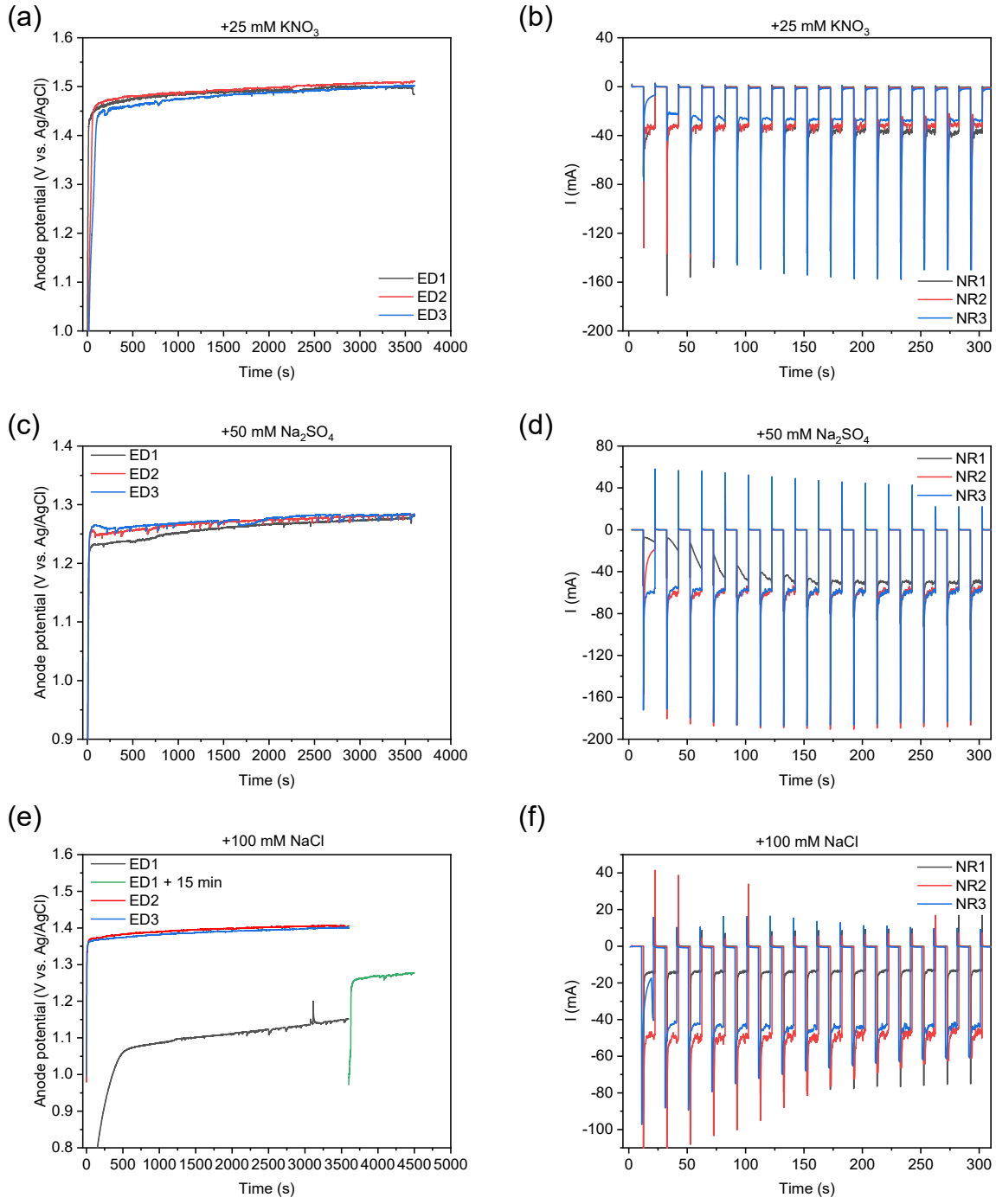

Figure S20. Chronopotentiometry and chronoamperometry data from EDNR experiments using different modified simulated wastewaters. (a) Anode (IrO_2-Ta_2O_5/Ti mesh electrode in the NH_3 synthesis chamber) potentials as functions of time in ED stages and **(b)** cathode (Ti electrode in the NH_3 synthesis chamber) current in the first 5 min into each NR stage in the EDNR experiment using NO_3^--laden simulated wastewater. **(c)** Anode (IrO_2-Ta_2O_5/Ti mesh electrode in the NH_3 synthesis chamber) potentials as functions of time in ED stages and **(d)** cathode (Ti electrode in the NH_3 synthesis chamber) current in the first 5 min into each NR stage in the EDNR experiment using SO_4^{2-}-laden simulated wastewater. **(e)** Anode (IrO_2-Ta_2O_5/Ti mesh electrode in the NH_3 synthesis chamber) potentials as functions of time in ED stages and **(f)** cathode (Ti electrode in the NH_3 synthesis chamber) current in the first 5 min into each NR stage in the EDNR experiment using Cl^--laden simulated wastewater. The average total current density from NR stages in all sets of experiments are given in **Fig. S21c**.

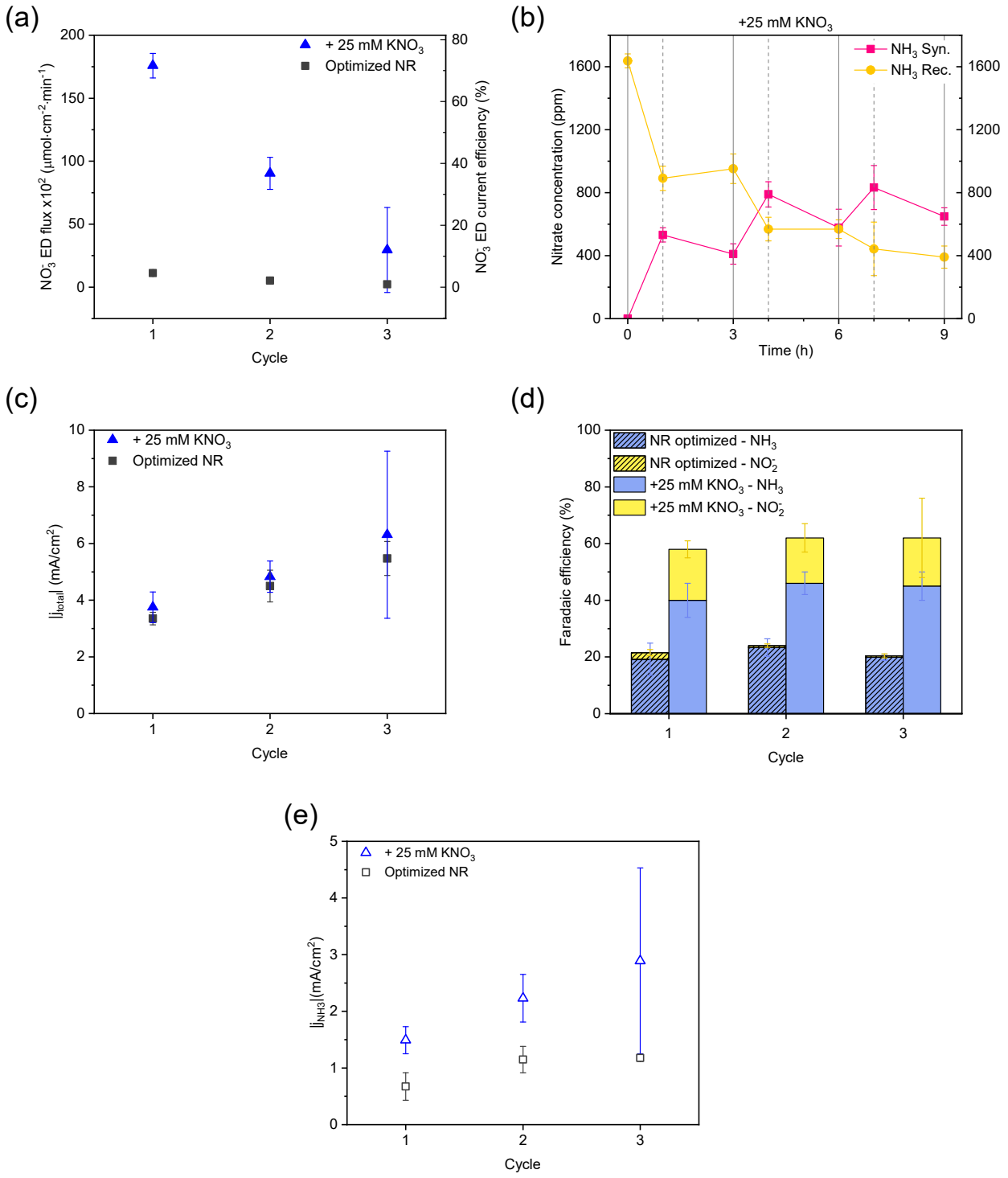

Figure S21. NO_3^--laden simulated wastewater EDNR. (a) NO_3^- ED flux (left y-axis) and NO_3^- ED current efficiency (right y-axis), **(b)** NO_3^- concentration trend (EDNR cycles are indicated by solid vertical lines and stages are indicated by dash vertical lines), **(c)** absolute value of total current density in NR stages, **(d)**

Faradaic efficiency in NR stages, and **(e)** absolute value of NH_3 partial current density in NR stages using NO_3^--laden simulated wastewater (+25 mM KNO_3): 13.9 mM $(NH_4)_2SO_4$ + 26.4 mM KNO_3, in comparison with baseline simulated wastewater (optimized NR) experiments. Error bars represent ± one standard deviation.

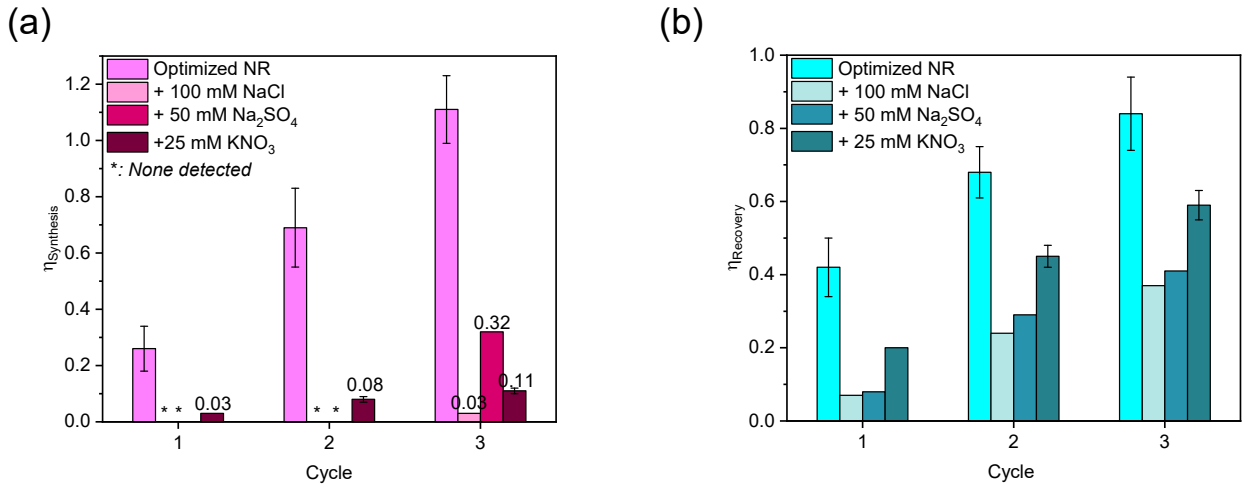

Figure S22. All influent effects. (a) NH_3 synthesis efficiency and **(b)** NH_3 recovery efficiency as functions of cycle number in EDNR experiments with a variety of influent conditions. Influents for the different scenarios are as follows. Baseline simulated wastewater (optimized NR): 13.9 mM $(NH_4)_2SO_4$ + 1.6 mM KNO_3. Cl^--laden (+100 mM NaCl): 13.9 mM $(NH_4)_2SO_4$ + 1.6 mM KNO_3 +100 mM NaCl. SO_4^{2-}-laden (+50 mM Na_2SO_4): 13.9 mM $(NH_4)_2SO_4$ + 1.6 mM KNO_3 + 50 mM Na_2SO_4. NO_3^--laden (+25 mM KNO_3): 13.9 mM $(NH_4)_2SO_4$ + 26.4 mM KNO_3. Error bars represent ± one standard deviation.

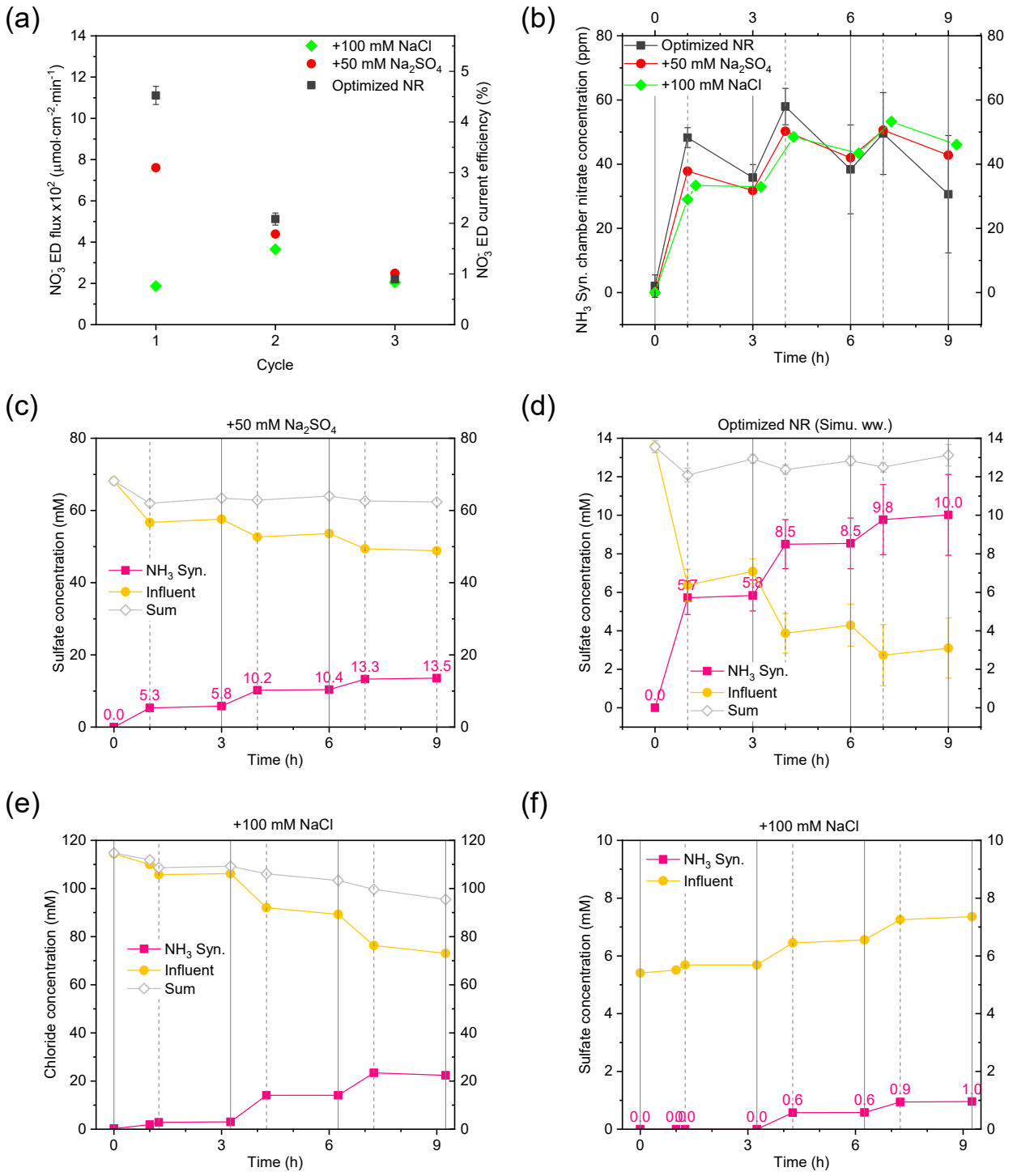

Figure S23. Influent anion effects on ED. (a) NO_3^- ED flux (left y-axis) and NO_3^- ED current efficiency (right y-axis) and **(b)** NH_3 synthesis chamber pH trend in EDNR experiments with various influent conditions. SO_4^{2-} concentration trends in EDNR experiments using **(c)** SO_4^{2-}-laden and **(d)** baseline simulated wastewaters. **(e)** Cl^- and **(f)** SO_4^{2-} concentration trends in EDNR experiments using Cl^--laden

simulated wastewater. EDNR cycles are indicated by solid vertical lines and stages are indicated by dash vertical lines. Error bars represent ± one standard deviation.

We observed that the total Cl^- concentration within the system decreased over time because the chlorine evolution reaction (CER) occurred at the NH_3 synthesis chamber IrO_2-Ta_2O_5/Ti mesh electrode during ED and at the influent chamber IrO_2-Ta_2O_5/Ti mesh electrode during NR, as a competitive process to water oxidation reaction (~17% decrease in sum Cl^- concentration after 3 cycles, accounting for 23% of total charge passed in ED + NR). Because CER does not produce protons, the NH_3 synthesis chamber pH at the end of ED1 was 3.2, much higher than in optimized NR. We had to extend the ED stage by 15 min in ED1 before starting NR, but it was still more alkaline than the optimal pH identified in earlier experiments (**Fig. S24b**). However, for ED2 and ED3, we were able to achieve favorable NH_3 synthesis chamber pH values using the same ED duration of 60 min.

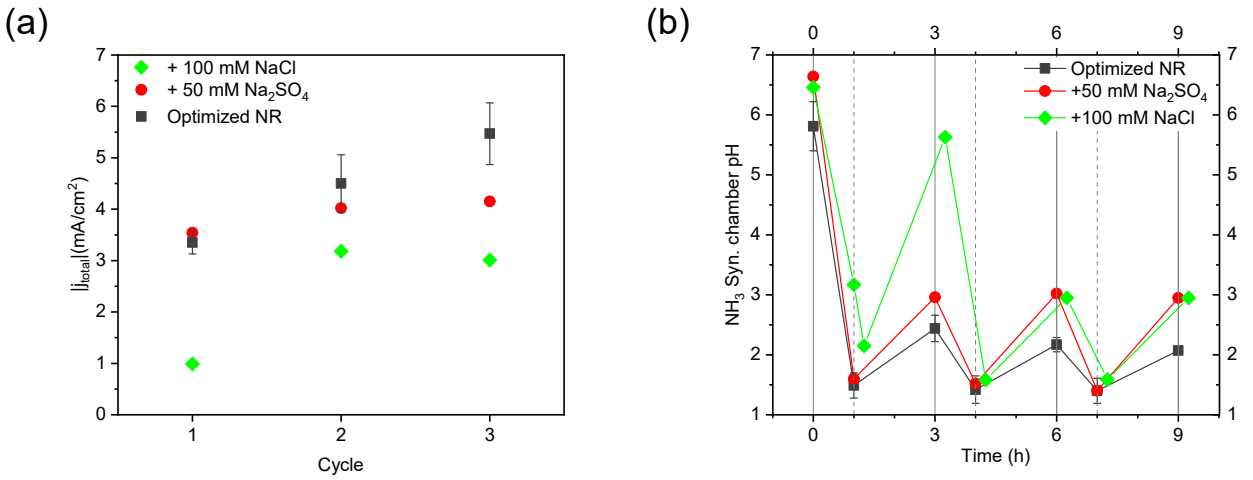

Figure S24. Influent anion effects on NR. (a) Absolute value of total current density in NR stages and **(b)** NH_3 synthesis chamber pH trend in EDNR experiments with a variety of influent conditions. EDNR cycles are indicated by solid vertical lines and stages are indicated by dash vertical lines. Error bars represent ± one standard deviation.

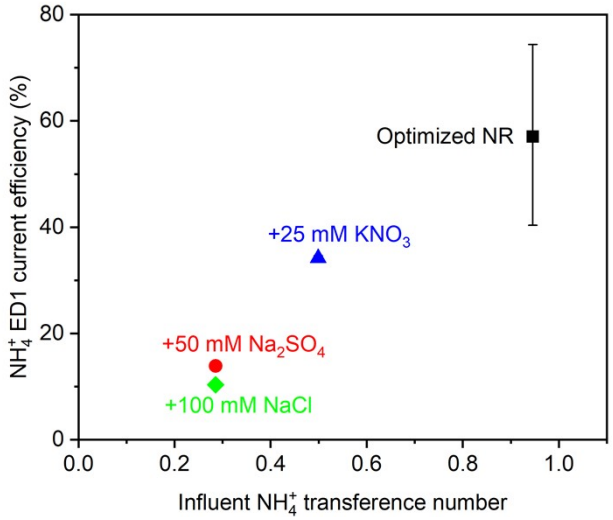

Figure S25. Influent cation effects on ED. NH_4^+ ED current efficiency in ED1 with a variety of influent conditions. Error bars represent ± one standard deviation.

Section S3.3.2 Real wastewaters

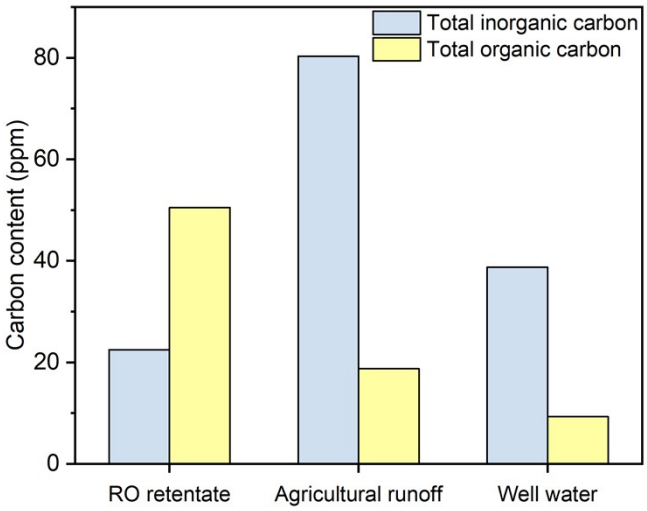

Figure S26. Total inorganic and organic carbon contents in different wastewaters used as influents in EDNR experiments. Triplicate or duplicate measurements were conducted for each sample, and the mean values are plotted.

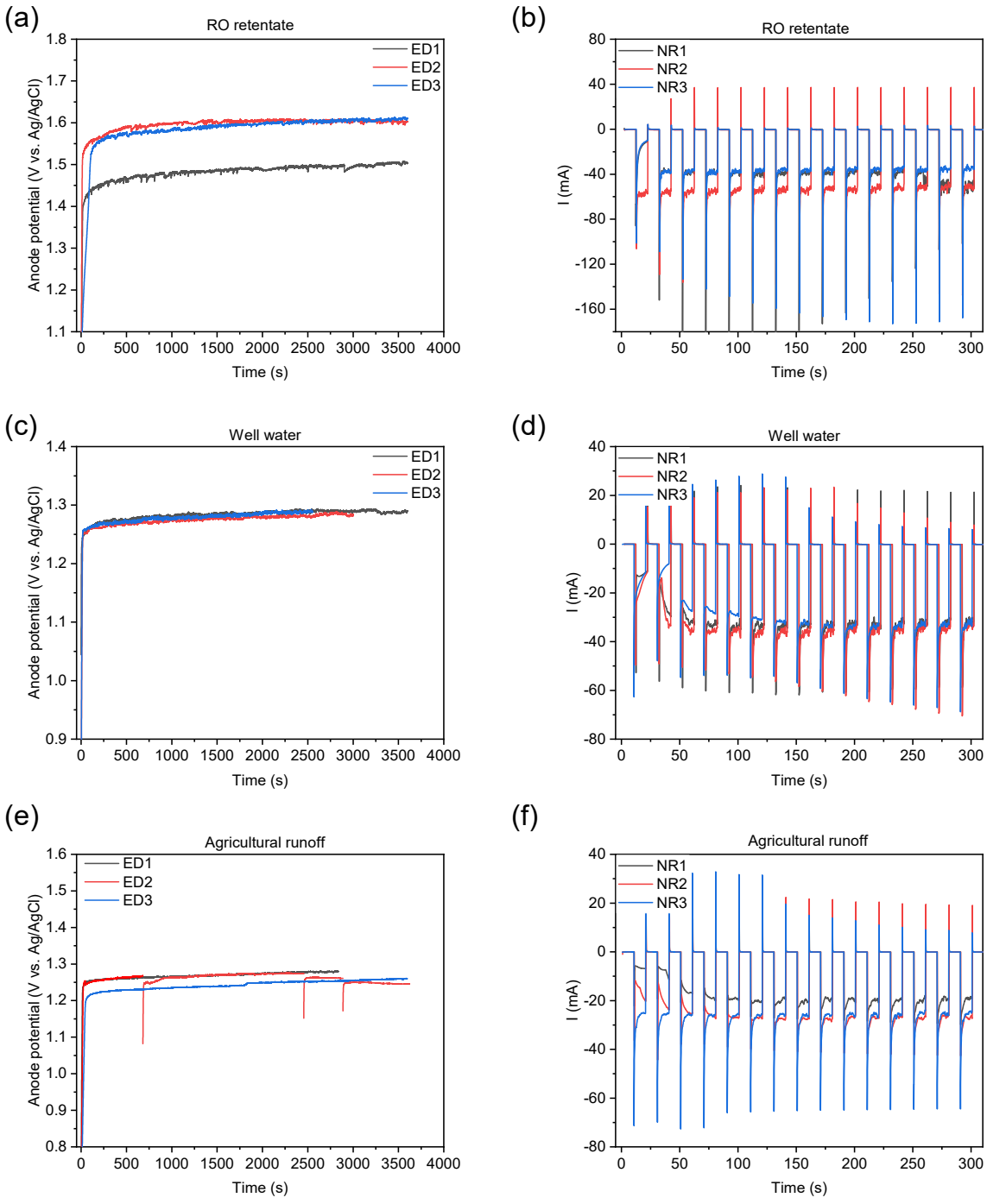

Figure S27. Chronopotentiometry and chronoamperometry data from EDNR experiments using different real wastewater influents. (a) Anode (IrO_2-Ta_2O_5/Ti mesh electrode in the NH_3 synthesis chamber) potentials as functions of time in ED stages and **(b)** cathode (Ti electrode in the NH_3 synthesis chamber) current in the first 5 min into each NR stage in the EDNR experiment using RO retentate. **(c)** Anode (IrO_2-Ta_2O_5/Ti mesh electrode in the NH_3 synthesis chamber) potentials as functions of time in ED

stages and **(d)** cathode (Ti electrode in the NH_3 synthesis chamber) current in the first 5 min into each NR stage in the EDNR experiment using well water. **(e)** Anode (IrO_2-Ta_2O_5/Ti mesh electrode in the NH_3 synthesis chamber) potentials as functions of time in ED stages and **(f)** cathode (Ti electrode in the NH_3 synthesis chamber) current in the first 5 min into each NR stage in the EDNR experiment using agricultural runoff. The average total current density from NR stages in all sets of experiments are given in **Fig. S29a**.

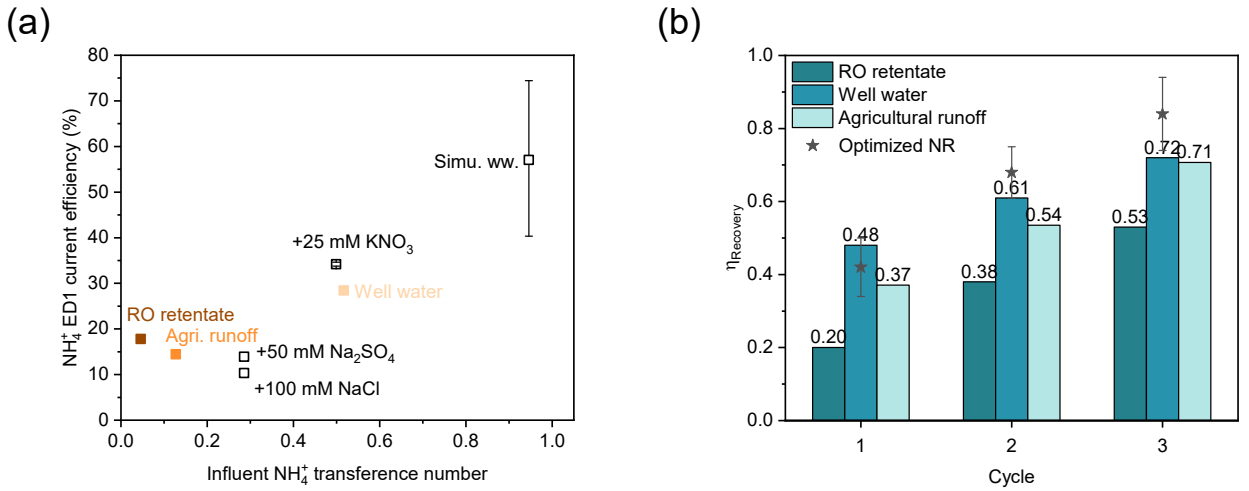

Figure S28. ED performance in EDNR experiments using different real wastewater influents. (a) NH_4^+ current efficiency in ED1, and (b) NH_3 recovery efficiency, in comparison with optimized NR experiments. Error bars represent ± one standard deviation for triplicate optimized NR experiments (all others n=1).

Similar to that observed in Cl^--laden experiment, the total amount of NO_2^- in the experiment using RO retentate decreased over time (20.5% of the initial amount) due to CER. Note that because some wastewater feedstocks contain nitrite, the definition of NH_3 synthesis efficiency ($\eta_{Synthesis}$) was revised to:

$$\eta_{\text{Synthesis, Cycle } i} = \frac{([NH_3]_{\text{Syn, NR}i} - [NH_3]_{\text{Syn, Ini}}) \times V_{Syn}}{([NO_3^-]_{\text{Inf, Ini}} + [NO_2^-]_{\text{Inf, Ini}}) \times V_{Inf}} \qquad \textbf{Eqn. S15}$$

where $[NH_3]_{\text{Syn, NR}i}$ is the NH_3 concentration in the NH_3 synthesis chamber at the end of the NR stage in EDNR cycle i, and $[NO_2^-]_{\text{Inf, Ini}}$ is the initial NO_2^- concentration in the influent before reaction starts. V_{Syn} is the electrolyte volume of the NH_3 synthesis chamber and its corresponding reservoir (50 mL), and V_{Inf} is the electrolyte volume of the influent chamber and its corresponding reservoir (50 mL).

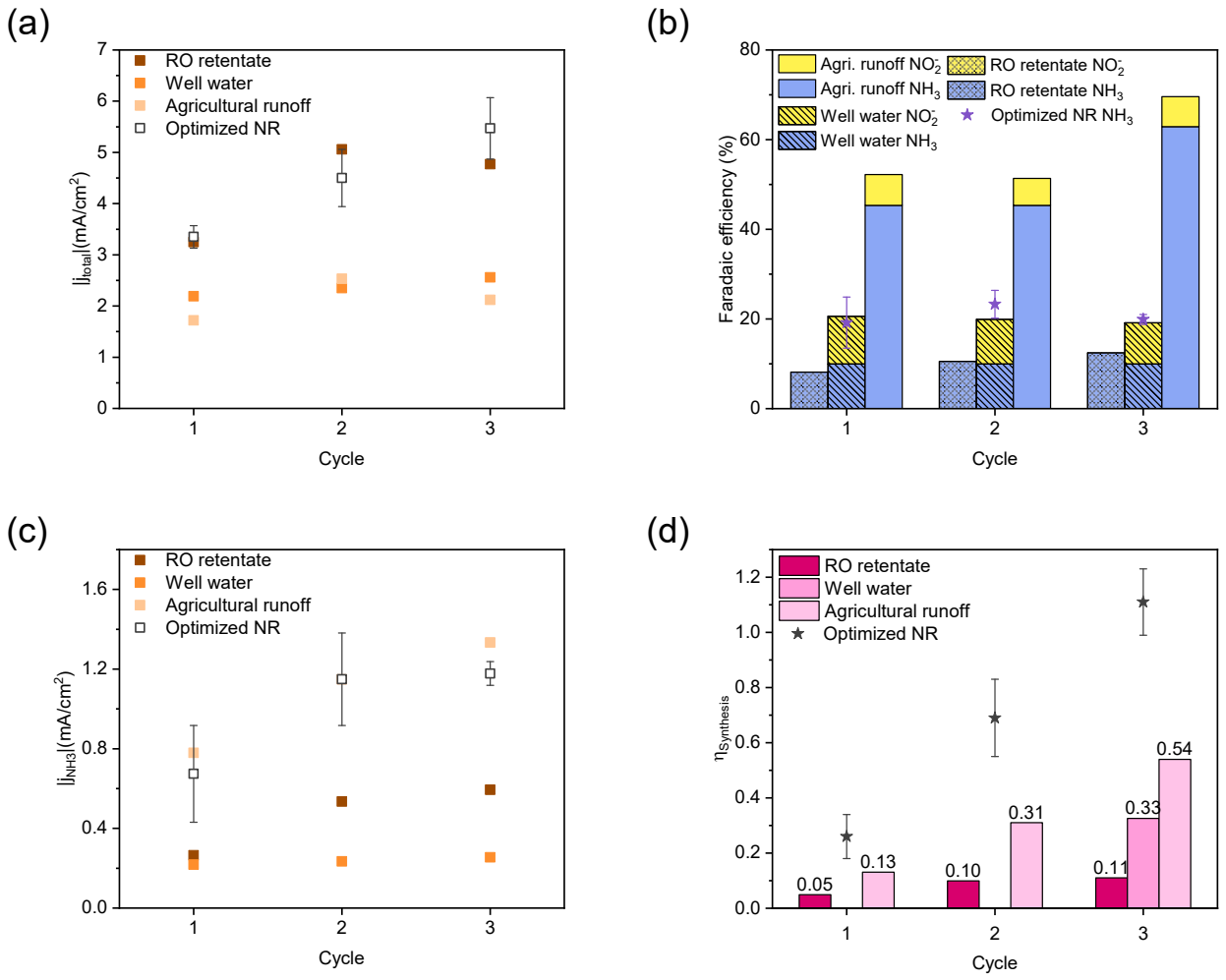

Figure S29. NR performance in EDNR experiments using different wastewater influents. (a) Absolute value of total current density, **(b)** Faradaic efficiency, **(c)** absolute value of NH_3 partial current density in NR stages, and **(d)** NH_3 synthesis efficiency, in comparison with optimized NR experiments. Error bars represent ± one standard deviation.

Note that in 4-cycle EDNR experiments using NH_4^+-enriched agricultural runoff influent, ED stage durations were shortened compared to the optimized NR experiments and varied between the two replicates to avoid full cell voltage overload (20 V). However, the total charge passed in all ED stages from the two replicates was almost identical (2% difference, **Figure S30a**).

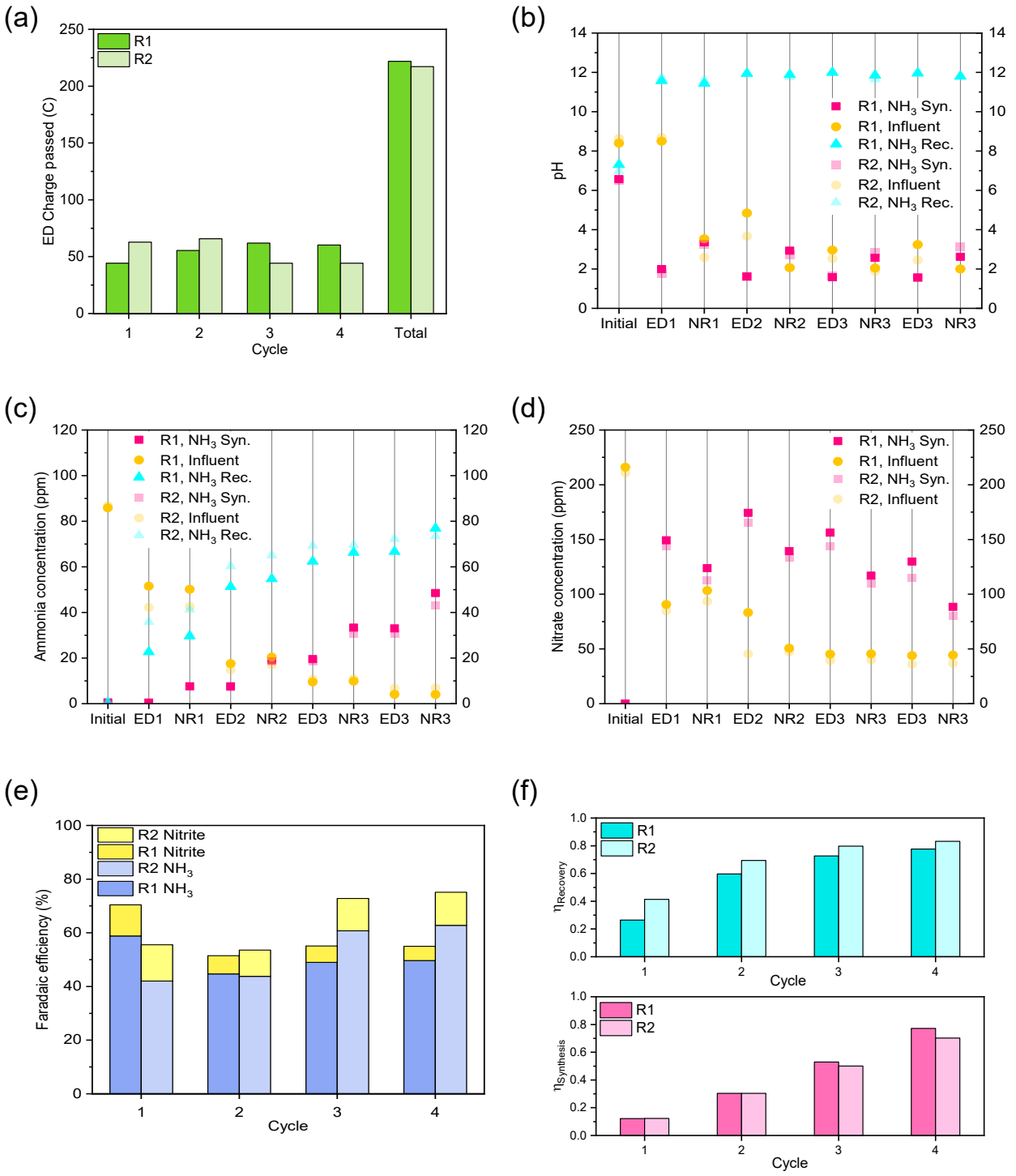

Figure S30. 4-cycle EDNR using NH_4^+-enriched agricultural runoff influent. Comparison of two replicate experiments **(a)** charge passed during ED stages, **(b)** pH trends, **(c)** NH_3 concentration trends, **(d)** NO_3^- concentration trends, **(e)** Faradaic efficiency during NR stages, and **(f)** NH_3 recovery (top panel) and synthesis efficiency (bottom panel). R1 and R2 represent Replicate #1 and Replicate #2, respectively.

Section S3.4 Long-term EDNR and product purification to treat agricultural runoff

In long-term experiments, the applied current density during ED stages was calculated using the average charge passed in corresponding stage from the 4-cycle EDNR experiments and 60 min ED duration. As a result, the magnitude of applied current was lower than in optimized NR, and we applied a higher electrolyte flow rate in ED stages to compensate for the decreased amount of charge passed (see **Section S3.2.3**).

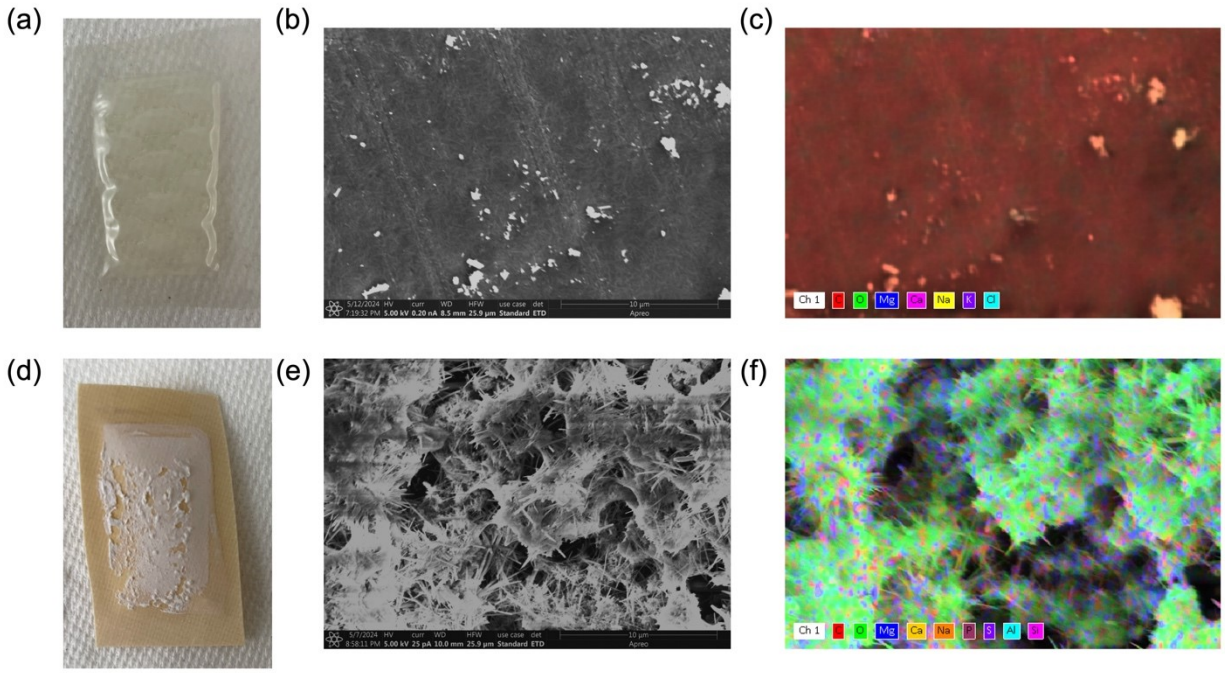

Figure S31. Membranes after long-term experiments. (a) Photo of the anion exchange membrane (the fouled side faced the NH_4^+-enriched agricultural runoff influent), **(b)** SEM image of the fouled side of the AEM, and **(c)** EDS of the same area. **(d)** Photo of the cation exchange membrane (the fouled side faced the NH_3 recovery chamber), **(e)** SEM image of the fouled side of the CEM, and **(f)** EDS of the same area. EDS chemical composition data from **(c)** and **(f)** are shown in **Table S6**.

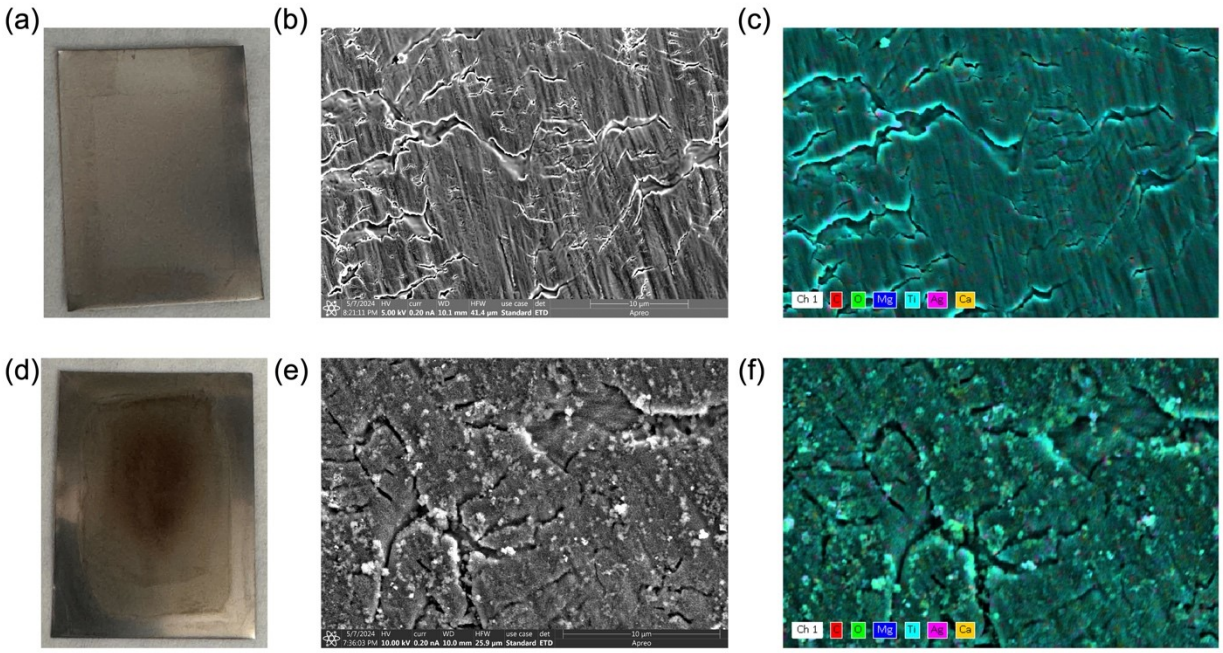

Figure S32. Ti electrode after long-term experiments. (a) Photo of the side of the Ti electrode that did not face the NH_3 synthesis chamber, **(b)** SEM image of the unused side of the Ti electrode, and **(c)** EDS of the same area. **(d)** Photo of the side of the Ti electrode that faced the NH_3 synthesis chamber electrolyte, **(e)** SEM image of the used side of the Ti electrode, and **(f)** EDS of the same area. ED chemical composition data from **(c)** and **(f)** are shown in **Table S6**.

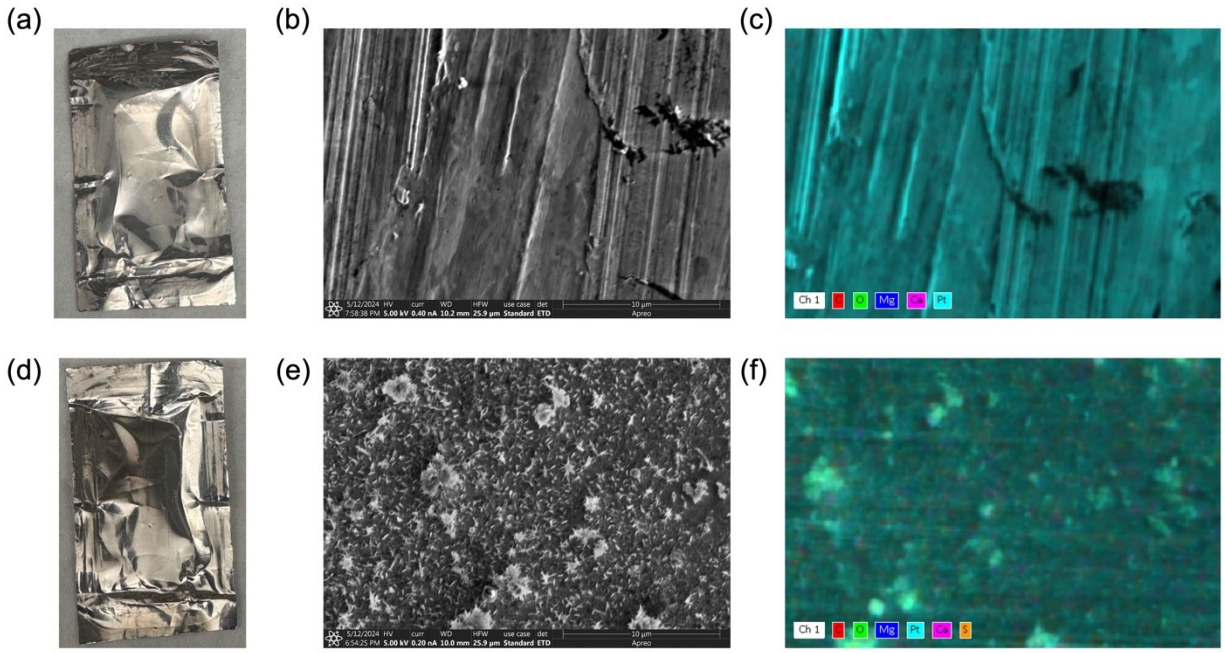

Figure S33. Pt electrode after long-term experiments. (a) Photo of the side of the Pt electrode that did not face the NH_3 recovery chamber, **(b)** SEM image of the unused side of the Pt electrode, and **(c)** EDS of the same area. **(d)** Photo of the side of the Pt electrode that faced the NH_3 synthesis chamber electrolyte, **(e)** SEM image of the used side of the Ti electrode, and **(f)** EDS of the same area. EDS chemical composition data from **(c)** and **(f)** are shown in **Table S6**.

Table S6 Chemical composition of electrodes and membranes from long-term EDNR experiment characterized by SEM-EDS

Element atomic %	C	O	Si	S	Cl	P	Na	Mg	K	Ca	Ti	Pt	Ag
Ti (unused side)	7.55	11.85	N.D.	0.01	N.D.	N.D.	0.01	N.D.	N.D.	0.03	80.51	N.D.	0.01
Ti (facing NH_3 synthesis chamber)	5.04	38.94	N.D.	0.07	0.03	0.05	0.24	0.94	0.02	0.09	54.17	N.D.	0.41
Pt (unused side)	66.02	8.69	N.D.	0.96	N.D.	N.D.	N.D.	N.D.	N.D.	0.03	N.D.	24.29	N.D.
Pt (facing NH_3 recovery chamber)	49.99	28.90	N.D.	0.68	N.D.	N.D.	0.02	1.73	N.D.	0.66	N.D.	18.03	N.D.
CEM (facing influent)	12.73	63.67	0.19	0.04	0.06	N.D.	0.10	9.36	N.D.	13.86	N.D.	N.D.	N.D.
AEM (facing NH_3 recovery chamber)	89.56	7.21	N.D.	N.D.	3.09	N.D.	0.06	0.04	N.D.	0.04	N.D.	N.D.	N.D.

*N.D. stands for not detected.

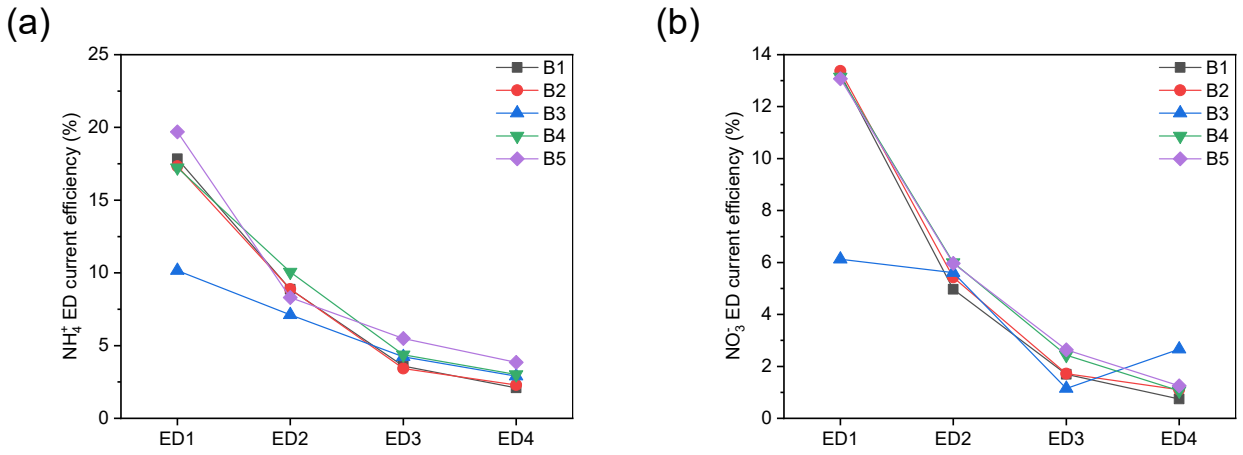

Figure S34. Long-term experiment ED. (a) NH_4^+ ED current efficiency and **(b)** NO_3^- ED current efficiency. B1–5 represents batch 1–5. The influent was NH_4^+-enriched agricultural runoff.

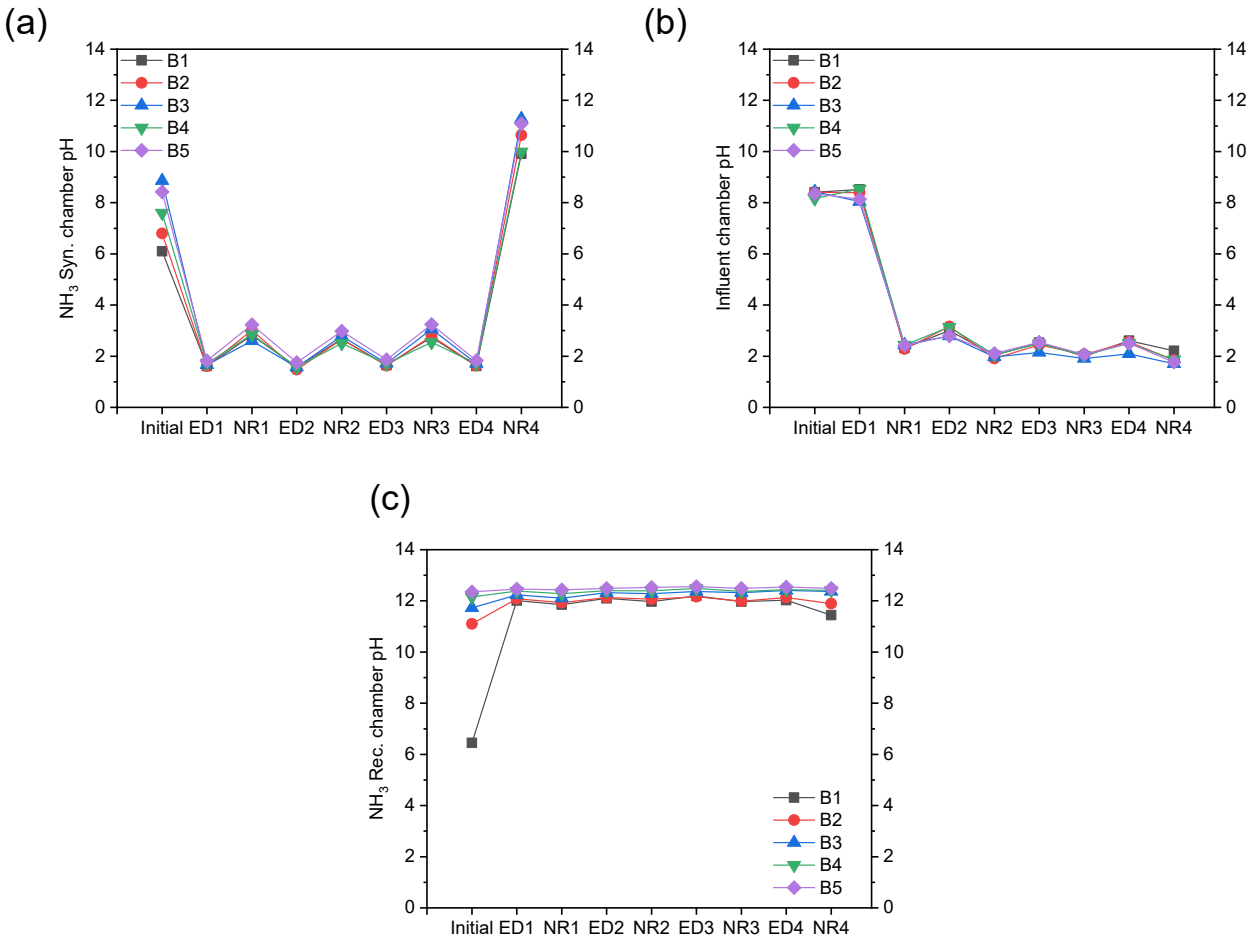

Figure S35. Long-term EDNR experiment pH. (a) NH_3 synthesis, **(b)** influent, and **(c)** NH_3 recovery chamber pH trends. B1–5 represents batch 1–5. The influent was NH_4^+-enriched agricultural runoff.

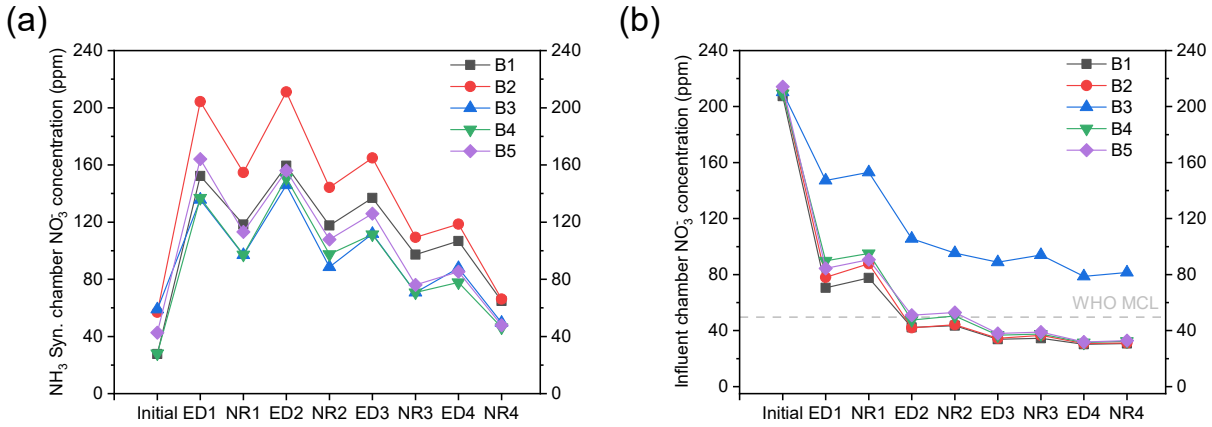

Figure S36. Long-term experiment NO_3^- concentrations. (a) NH_3 synthesis and **(b)** influent chamber NO_3^- concentration trends. Dashed line represents MCL for NO_3^- in drinking water set by the World Health Organization (10 ppm NO_3^--N).[2] B1–5 represents batch 1–5. The influent was NH_4^+-enriched agricultural runoff.

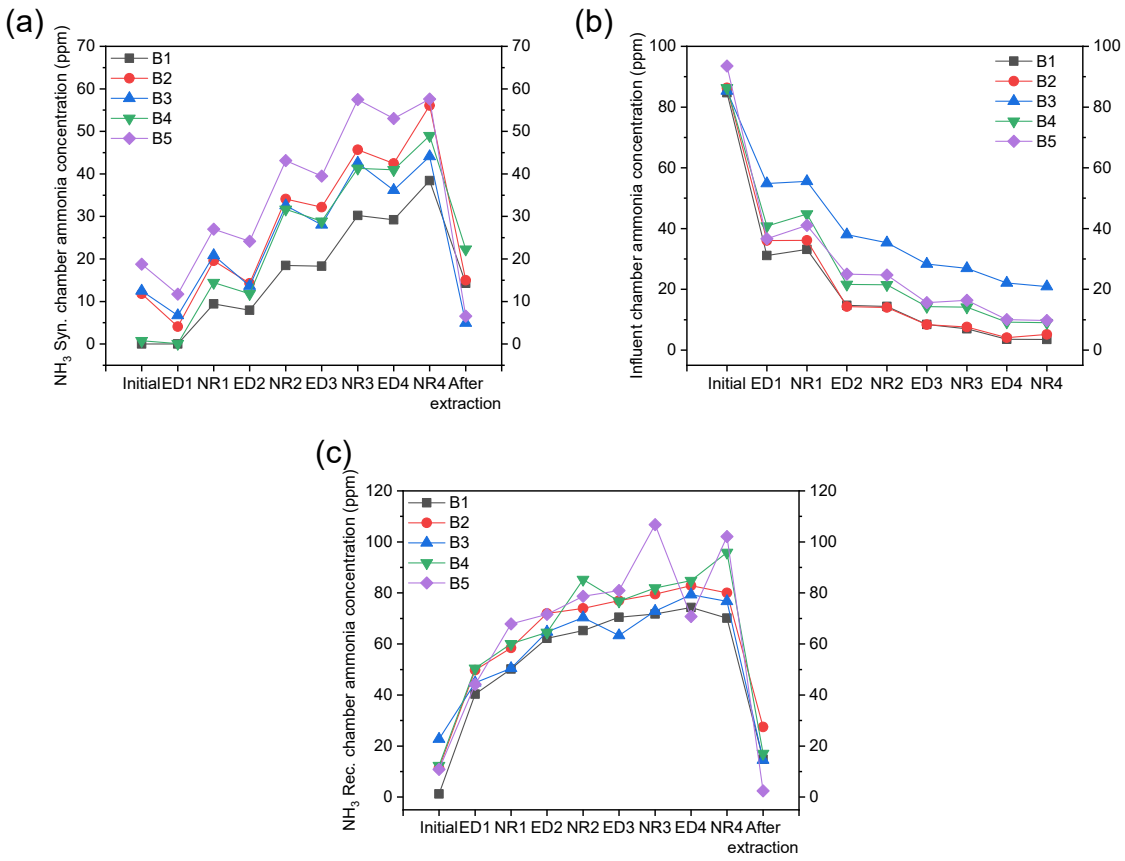

Figure S37. Long-term experiment NH_3 concentrations. (a) NH_3 synthesis, **(b)** influent, and **(c)** NH_3 recovery chamber NH_3 concentration. B1–5 represents batch 1–5. Influent was NH_4^+-enriched agricultural runoff.

Table S7 Concentrations of Na^+ and ClO_4^- in the initial and final samples of the long-term EDNR experiment

	NH_3 synthesis chamber	Influent chamber (Agricultural runoff)	NH_3 recovery chamber
Initial Na^+ conc. before long-term EDNR started	1072.7±24.0 mM*	6.6 mM	1072.7±24.0 mM*
Final Na^+ conc. after the last batch of long-term EDNR (batch 5)	799.5 mM	9.5 mM	732.3 mM
Initial ClO_4^- conc. before long-term EDNR started	968.0±12.1 mM#	0	968.0±12.1 mM#
Final ClO_4^- conc. after the last batch of long-term EDNR (batch 5)	1151.1 mM	25.0 mM	896.3 mM

* Measured using the 1 M $NaClO_4$ stock solution, ± represents standard deviations from triplicate measurements.

Measured using the 1 M $NaClO_4$ stock solution, ± represents standard deviations from triplicate measurements.

We noted that a significant portion of Na^+ was lost from both NH_3 synthesis and NH_3 recovery chambers after the long-term EDNR experiment, likely due to several factors. For both chambers, because a large dilution factor (1000 times) was used in preparing liquid samples for cation chromatography measurements, the measurement variance was high (24 mM in measuring the 1 M $NaClO_4$ stock solution) and account for *ca.* 7–9% of the Na^+ loss. For the NH_3 recovery chamber, Na^+ diffused (during ED stages) and migrated (during NR stages) across the CEM into the influent over five batches (up to 17.5 mM), while a large portion of Na^+ could be incorporated into the CEM during such movement (*ca.* 140 mM, calculated based on the CEM ion exchange capacity). For the NH_3 synthesis chamber, Na^+ could be incorporated into the AEM due to its imperfect co-ion exclusion, especially in electrolyte concentrations comparable to the membrane fixed charge density based on Donnan theory (uptake ≥ 50% in electrolytes with ≥ 0.89 M Na^+[22]). Meanwhile, we observed that after the long-term EDNR experiment, there was an additional 2.5 mM Ca^{2+} and 49 mM Mg^{2+} in the NH_3 recovery chamber, and an additional 7 mM K^+ in the NH_3 synthesis chamber.

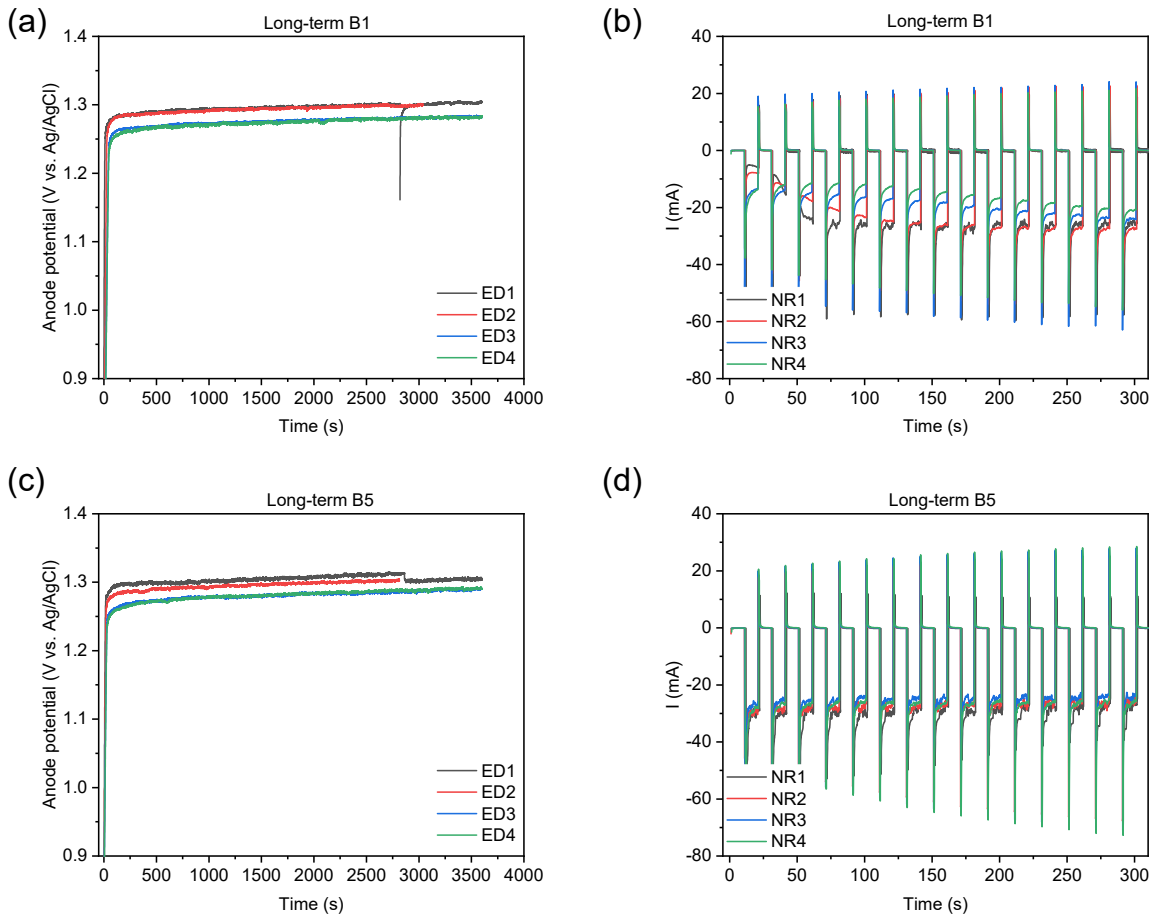

Figure S38. Chronopotentiometry and chronoamperometry data from long-term EDNR experiments. (a) Anode (IrO_2-Ta_2O_5/Ti mesh electrode in the NH_3 synthesis chamber) potentials as functions of time in ED stages and **(b)** cathode (Ti electrode in the NH_3 synthesis chamber) current in the first 5 min into each NR stage in long-term EDNR batch 1. **(c)** Anode (IrO_2-Ta_2O_5/Ti mesh electrode in the NH_3 synthesis chamber) potentials as functions of time in ED stages and **(d)** cathode (Ti electrode in the NH_3 synthesis chamber) current in the first 5 min into each NR stage in long-term EDNR batch 5. The average total current density from NR stages in all sets of experiments are given in **Fig. S39**.

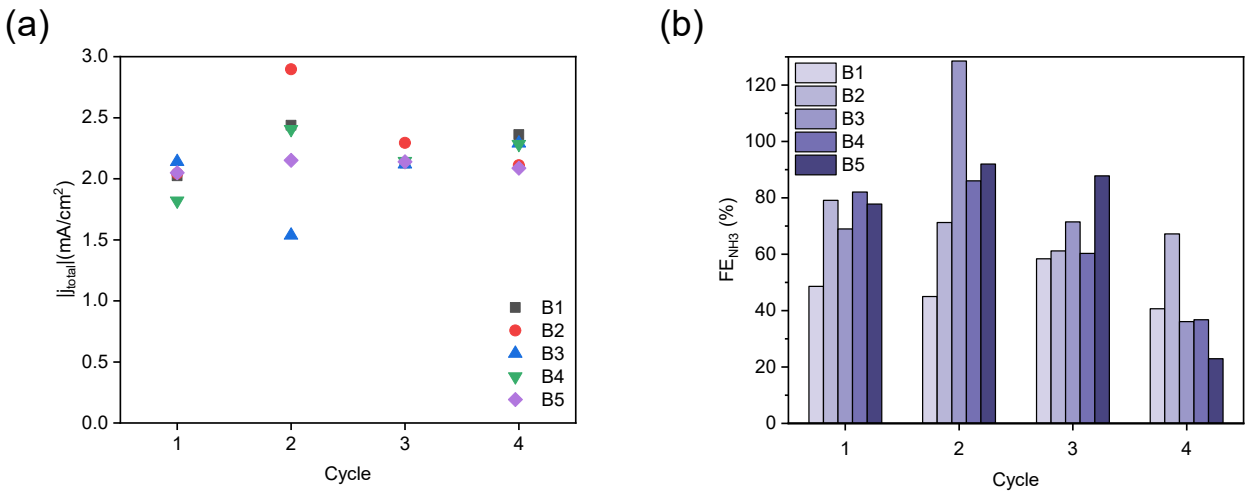

Figure S39. Long-term experiment NR performance. (a) Absolute value of total current density and **(b)** NH_3 Faradaic efficiency in NR stages. B1–5 represents batch 1–5. The influent was NH_4^+-enriched agricultural runoff.

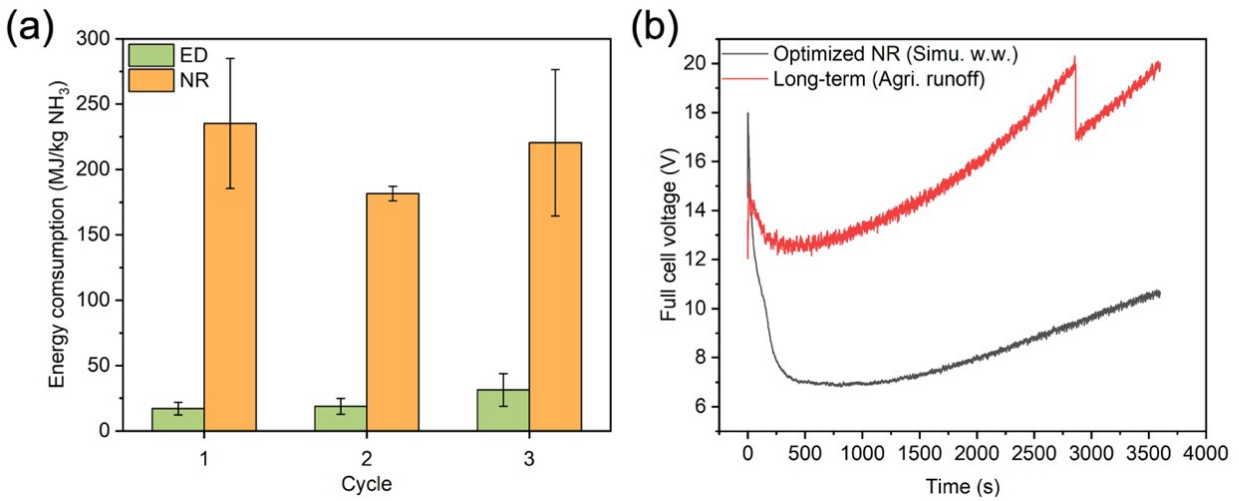

Figure S40. Energy consumption comparison. (a) Energy consumption from ED and NR stages in optimized NR experiments using simulated wastewater influent. Error bars represent ± one standard deviation. **(b)** Comparison of full cell voltage in ED1 from one optimized NR replicate and ED1 from B5 of long-term EDNR experiment.

Table S8 Energy consumption in electrochemical NH_3 manufacturing technologies using feedstocks with environmentally relevant Nr concentrations

Electrochemical technology	**Feedstock**	**Feedstock Nr level**	**Product separation**	**Product**	**Energy consumption**
Bipolar electrodialysis stack[23]	Synthetic wastewater	18.7 mM NH_3	Membrane stripping	$(NH_4)_2SO_4$ and H_2SO_4 mixture with pH 3 (concentration not reported)	18.3 MJ/kg NH_3-N
Electrochemical ammonia accumulation[24]	Livestock wastewater	178–214 mM NH_3	None	1.26 M NH_3 and 0.5 M Na_2SO_4 mixture	101.5 MJ/kg NH_3-N
Hydrophobic membrane coated cathode[25]	Synthetic anaerobic concentrate	71.4 mM NH_3	Membrane stripping	44.6 mM NH_3 and 50 mM H_3PO_4, Na_2HPO_4 mixture	57.6 MJ/kg NH_3-N
Electrodialysis-electrochemical ammonia stripping[26]	Anaerobic digestate	100.3 mM NH_3	Membrane stripping	237.8 mM NH_3 as $NH_4H_2PO_4$ and $(NH_4)_2HPO_4$ mixture	50.7 MJ/kg NH_3-N
Integrated flow-electrode capacitive deionization and flow cathode system[27]	Simulated groundwater	2.2 mM NO_3^-	Membrane stripping	0.5 mM $(NH_4)_2SO_4$ and 0.5 M H_2SO_4 mixture	31400 MJ/kg NH_3-N
Bifunctional nitrate adsorption-reduction electrode	Agricultural tile drainage water	0.27 mM NO_3^-	None	2.0 mM NH_3 in the feedstock mixture	904.7 MJ/kg NH_3-N
Concurrent electrocatalysis and membrane extraction[28,29]	Synthetic wastewater	20 mM NO_3^-	Membrane stripping	38 mM $(NH_4)_2SO_4$ and 62 mM H_2SO_4 mixture	644.4 MJ/kg NH_3-N
Electrified membrane[30]	Synthetic wastewater	25 mM NO_3^-	Membrane stripping	10 mM $(NH_4)_2SO_4$ and 0.5 M acidified Na_2SO_4 mixture	1962 MJ/kg NH_3-N
Membrane-free alkaline electrolyzer[31]	KNO_3 solution	7.14 mM NO_3^-	Water absorption at 5 °C	4.12 M NH_3 solution	168.2 MJ/kg NH_3-N
Integrated nitrate reduction and electrochemical stripping[32]	Mixture of real secondary effluent and RO brine	2.0 mM NO_3^-	Electrochemical stripping	1.3 mM $(NH_4)_2SO_4$ and 0.1 M H_2SO_4 mixture	1224 MJ/kg NH_3-N
EDNR (This work)	Synthetic wastewater	27.8 mM NH_4^+ + 1.6 mM NO_3^-	None	In 1 M $NaClO_4$	245 MJ/kg NH_3-N
EDNR (This work)	NH_4^+-enriched agricultural runoff	4.8 mM NH_4^+ + 3.3 mM NO_3^-	Membrane stripping	101 mM NH_3 as $NH_4H_2PO_4$ and $(NH_4)_2HPO_4$ mixture	920 MJ/kg NH_3-N

In addition to the discussion around energy consumption provided in the main manuscript, we would like to comment on the cost aspect as well. The EDNR process employs electrodialysis to separate NH_4^+ and NO_3^- from polluted wastewater influent and reactions to recover NH_3 from NH_4^+ (using OH^- generated from water reduction reaction) and synthesize NH_3 from NO_3^- (nitrate reduction reaction). For the reaction step (NR), there has not been commercialized systems to compare with to the authors' knowledge. For the separation step (ED), a commercialized and popular technique to separate NH_4^+ and NO_3^- from wastewater is ion exchange. Although the adsorption process itself consumes very little energy, the ion exchange resins need to be regenerated often with concentrated acid, base, or salt solutions, which leads to secondary waste. The cost of purchasing these chemicals to regenerate the ion exchange resins contributes to 30-55% of all operating cost of a proposed plant using municipal wastewater influent.[33,34] It is hard to draw a direct comparison of cost per NH_3 produced between EDNR and commercialized ion exchange technologies because the EDNR process is still at bench-scale and under development. But there are several advantages of EDNR that could possibly reduce the cost compared to the ion exchange system: (1) uses electrical field as the driving force for NH_4^+ and NO_3^- separation and avoids the usage of chemicals and their associated transportation cost, (2) can operate continuously and avoids the off time needed for resin regeneration, and (3) doesn't generate secondary waste stream from regeneration that needs to be processed. Although cost is out of scope of the current work, we plan to conduct future work on developing a techno-economic analysis model of the EDNR process.

In future efforts to scale up the EDNR process, we note that H_2 is generated as a side product. Although it might require additional engineering strategies to manage its related safety hazard, it can also be collected as a profitable product stream.

References

(1) O'Dell, J. W. DETERMINATION OF AMMONIA NITROGEN BY SEMI-AUTOMATED COLORIMETRY. In *Methods for the Determination of Metals in Environmental Samples*; Elsevier, 1996; pp 434–448. https://doi.org/10.1016/B978-0-8155-1398-8.50024-0.

(2) Ward, M. H.; Jones, R. R.; Brender, J. D.; de Kok, T. M.; Weyer, P. J.; Nolan, B. T.; Villanueva, C. M.; van Breda, S. G. Drinking Water Nitrate and Human Health: An Updated Review. *Int J Environ Res Public Health* **2018**, *15* (7), 1557. https://doi.org/10.3390/ijerph15071557.

(3) McEnaney, J. M.; Blair, S. J.; Nielander, A. C.; Schwalbe, J. A.; Koshy, D. M.; Cargnello, M.; Jaramillo, T. F. Electrolyte Engineering for Efficient Electrochemical Nitrate Reduction to Ammonia on a Titanium Electrode. *ACS Sustainable Chem. Eng.* **2020**, *8* (7), 2672–2681. https://doi.org/10.1021/acssuschemeng.9b05983.

(4) Wu, Z.-Y.; Karamad, M.; Yong, X.; Huang, Q.; Cullen, D. A.; Zhu, P.; Xia, C.; Xiao, Q.; Shakouri, M.; Chen, F.-Y.; Kim, J. Y. (Timothy); Xia, Y.; Heck, K.; Hu, Y.; Wong, M. S.; Li, Q.; Gates, I.; Siahrostami, S.; Wang, H. Electrochemical Ammonia Synthesis via Nitrate Reduction on Fe Single Atom Catalyst. *Nat Commun* **2021**, *12* (1), 2870. https://doi.org/10.1038/s41467-021-23115-x.

(5) Gao, Q.; Pillai, H. S.; Huang, Y.; Liu, S.; Mu, Q.; Han, X.; Yan, Z.; Zhou, H.; He, Q.; Xin, H.; Zhu, H. Breaking Adsorption-Energy Scaling Limitations of Electrocatalytic Nitrate Reduction on Intermetallic CuPd Nanocubes by Machine-Learned Insights. *Nat Commun* **2022**, *13* (1), 2338. https://doi.org/10.1038/s41467-022-29926-w.

(6) Murphy, E.; Liu, Y.; Matanovic, I.; Guo, S.; Tieu, P.; Huang, Y.; Ly, A.; Das, S.; Zenyuk, I.; Pan, X.; Spoerke, E.; Atanassov, P. Highly Durable and Selective Fe- and Mo-Based Atomically Dispersed Electrocatalysts for Nitrate Reduction to Ammonia via Distinct and Synergized NO2– Pathways. *ACS Catal.* **2022**, 6651–6662. https://doi.org/10.1021/acscatal.2c01367.

(7) Crawford, J.; Yin, H.; Du, A.; O'Mullane, A. P. Nitrate-to-Ammonia Conversion at an InSn-Enriched Liquid-Metal Electrode. *Angewandte Chemie* **2022**, *134* (23), e202201604. https://doi.org/10.1002/ange.202201604.

(8) Wang, Y.; Xu, A.; Wang, Z.; Huang, L.; Li, J.; Li, F.; Wicks, J.; Luo, M.; Nam, D.-H.; Tan, C.-S.; Ding, Y.; Wu, J.; Lum, Y.; Dinh, C.-T.; Sinton, D.; Zheng, G.; Sargent, E. H. Enhanced Nitrate-to-Ammonia Activity on Copper–Nickel Alloys via Tuning of Intermediate Adsorption. *J. Am. Chem. Soc.* **2020**, *142* (12), 5702–5708. https://doi.org/10.1021/jacs.9b13347.

(9) Chen, F.-Y.; Wu, Z.-Y.; Gupta, S.; Rivera, D. J.; Lambeets, S. V.; Pecaut, S.; Kim, J. Y. T.; Zhu, P.; Finfrock, Y. Z.; Meira, D. M.; King, G.; Gao, G.; Xu, W.; Cullen, D. A.; Zhou, H.; Han, Y.; Perea, D. E.; Muhich, C. L.; Wang, H. Efficient Conversion of Low-Concentration Nitrate Sources into Ammonia on a Ru-Dispersed Cu Nanowire Electrocatalyst. *Nat. Nanotechnol.* **2022**, 1–9. https://doi.org/10.1038/s41565-022-01121-4.

(10) Katsounaros, I.; Kyriacou, G. Influence of the Concentration and the Nature of the Supporting Electrolyte on the Electrochemical Reduction of Nitrate on Tin Cathode. *Electrochimica Acta* **2007**, *52* (23), 6412–6420. https://doi.org/10.1016/j.electacta.2007.04.050.

(11) Wang, Y.; Li, H.; Zhou, W.; Zhang, X.; Zhang, B.; Yu, Y. Structurally Disordered RuO2 Nanosheets with Rich Oxygen Vacancies for Enhanced Nitrate Electroreduction to Ammonia. *Angewandte Chemie* **2022**, *134* (19), e202202604. https://doi.org/10.1002/ange.202202604.
(12) Guo, J.; Brimley, P.; Liu, M. J.; Corson, E. R.; Muñoz, C.; Smith, W. A.; Tarpeh, W. A. Mass Transport Modifies the Interfacial Electrolyte to Influence Electrochemical Nitrate Reduction. *ACS Sustainable Chem. Eng.* **2023**, *11* (20), 7882–7893. https://doi.org/10.1021/acssuschemeng.3c01057.
(13) Zhong, C.; Deng, Y.; Hu, W.; Qiao, J.; Zhang, L.; Zhang, J. A Review of Electrolyte Materials and Compositions for Electrochemical Supercapacitors. *Chemical Society Reviews* **2015**, *44* (21), 7484–7539. https://doi.org/10.1039/C5CS00303B.
(14) Jackson, M. N.; Jung, O.; Lamotte, H. C.; Surendranath, Y. Donor-Dependent Promotion of Interfacial Proton-Coupled Electron Transfer in Aqueous Electrocatalysis. *ACS Catal.* **2019**, *9* (4), 3737–3743. https://doi.org/10.1021/acscatal.9b00056.
(15) Da Silva, S.; Basséguy, R.; Bergel, A. Electrochemical Deprotonation of Phosphate on Stainless Steel. *Electrochimica Acta* **2004**, *49* (26), 4553–4561. https://doi.org/10.1016/j.electacta.2004.04.039.
(16) Marcandalli, G.; Boterman, K.; Koper, M. T. M. Understanding Hydrogen Evolution Reaction in Bicarbonate Buffer. *Journal of Catalysis* **2022**, *405*, 346–354. https://doi.org/10.1016/j.jcat.2021.12.012.
(17) Lim, J.; Liu, C.-Y.; Park, J.; Liu, Y.-H.; Senftle, T. P.; Lee, S. W.; Hatzell, M. C. Structure Sensitivity of Pd Facets for Enhanced Electrochemical Nitrate Reduction to Ammonia. *ACS Catal.* **2021**, *11* (12), 7568–7577. https://doi.org/10.1021/acscatal.1c01413.
(18) Liu, M. J.; Guo, J.; Hoffman, A. S.; Stenlid, J. H.; Tang, M. T.; Corson, E. R.; Stone, K. H.; Abild-Pedersen, F.; Bare, S. R.; Tarpeh, W. A. Catalytic Performance and Near-Surface X-Ray Characterization of Titanium Hydride Electrodes for the Electrochemical Nitrate Reduction Reaction. *J. Am. Chem. Soc.* **2022**, *144* (13), 5739–5744. https://doi.org/10.1021/jacs.2c01274.
(19) *CXM-200 (CMI-7000) Cation Exchange Membranes | Technical Specifications*. Membranes International Inc. https://ionexchangemembranes.com/cmi-7000-cation-exchange-membranes-technical-specifications/ (accessed 2024-02-06).
(20) Kim, J. M.; Lin, Y.; Hunter, B.; Beckingham, B. S. Transport and Co-Transport of Carboxylate Ions and Ethanol in Anion Exchange Membranes. *Polymers* **2021**, *13* (17), 2885. https://doi.org/10.3390/polym13172885.
(21) Rosenberg, N. W.; Tirrell, C. E. Limiting Currents in Membrane Cells. *Ind. Eng. Chem.* **1957**, *49* (4), 780–784. https://doi.org/10.1021/ie50568a047.
(22) El-Nagar, G. A.; Haun, F.; Gupta, S.; Stojkovikj, S.; Mayer, M. T. Unintended Cation Crossover Influences CO2 Reduction Selectivity in Cu-Based Zero-Gap Electrolysers. *Nat Commun* **2023**, *14* (1), 2062. https://doi.org/10.1038/s41467-023-37520-x.
(23) Rodrigues, M.; de Mattos, T. T.; Sleutels, T.; ter Heijne, A.; Hamelers, H. V. M.; Buisman, C. J. N.; Kuntke, P. Minimal Bipolar Membrane Cell Configuration for Scaling Up Ammonium Recovery. *ACS Sustainable Chem. Eng.* **2020**, *8* (47), 17359–17367. https://doi.org/10.1021/acssuschemeng.0c05043.
(24) Lee, G.; Kim, K.; Chung, J.; Han, J.-I. Electrochemical Ammonia Accumulation and Recovery from Ammonia-Rich Livestock Wastewater. *Chemosphere* **2021**, *270*, 128631. https://doi.org/10.1016/j.chemosphere.2020.128631.

(25) Kim, K.-Y.; Moreno-Jimenez, D. A.; Efstathiadis, H. Electrochemical Ammonia Recovery from Anaerobic Centrate Using a Nickel-Functionalized Activated Carbon Membrane Electrode. *Environ. Sci. Technol.* **2021**, *55* (11), 7674–7680. https://doi.org/10.1021/acs.est.1c01703.
(26) Aung, S. L.; Choi, J.; Cha, H.; Woo, G.; Song, K. G. Ammonia-Selective Recovery from Anaerobic Digestate Using Electrochemical Ammonia Stripping Combined with Electrodialysis. *Chemical Engineering Journal* **2024**, *479*, 147949. https://doi.org/10.1016/j.cej.2023.147949.
(27) Sun, J.; Garg, S.; Waite, T. D. A Novel Integrated Flow-Electrode Capacitive Deionization and Flow Cathode System for Nitrate Removal and Ammonia Generation from Simulated Groundwater. *Environ. Sci. Technol.* **2023**. https://doi.org/10.1021/acs.est.3c03922.
(28) Shi, N.; Gao, J.; Li, K.; Li, Y.; Zhang, W.; Yang, Q.; Jiang, B. Upcycling Wastewater Nitrate into Ammonia Fertilizer via Concurrent Electrocatalysis and Membrane Extraction. *Chemical Engineering Journal* **2023**, *455*, 140959. https://doi.org/10.1016/j.cej.2022.140959.
(29) Kim, K.; Zagalskaya, A.; Ng, J. L.; Hong, J.; Alexandrov, V.; Pham, T. A.; Su, X. Coupling Nitrate Capture with Ammonia Production through Bifunctional Redox-Electrodes. *Nat Commun* **2023**, *14* (1), 823. https://doi.org/10.1038/s41467-023-36318-1.
(30) Gao, J.; Shi, N.; Li, Y.; Jiang, B.; Marhaba, T.; Zhang, W. Electrocatalytic Upcycling of Nitrate Wastewater into an Ammonia Fertilizer via an Electrified Membrane. *Environ. Sci. Technol.* **2022**. https://doi.org/10.1021/acs.est.1c08442.
(31) Chen, Y.; Ammari-Azar, P.; Liu, H.; Lee, J.; Xi, Y.; Castellano, M. J.; Gu, S.; Li, W. Sustainable Waste-Nitrogen Upcycling Enabled by Low-Concentration Nitrate Electrodialysis and High-Performance Ammonia Electrosynthesis. *EES. Catal.* **2023**, *1* (4), 504–515. https://doi.org/10.1039/D3EY00058C.
(32) Liu, M. J.; Miller, D. M.; Tarpeh, W. A. Reactive Separation of Ammonia from Wastewater Nitrate via Molecular Electrocatalysis. *Environ. Sci. Technol. Lett.* **2023**, *10* (5), 458–463. https://doi.org/10.1021/acs.estlett.3c00205.
(33) Mayor, Á.; Vinardell, S.; Ganesan, K.; Bacardí, C.; Cortina, J. L.; Valderrama, C. Life-Cycle Assessment and Techno-Economic Evaluation of the Value Chain in Nutrient Recovery from Wastewater Treatment Plants for Agricultural Application. *Science of The Total Environment* **2023**, *892*, 164452. https://doi.org/10.1016/j.scitotenv.2023.164452.
(34) Reboredo Bonilla, D. Techno-Economic Evaluation of Ion Exchange Technologies to Recover Nitrogen and Phosphorus from Municipal Wastewater. Master thesis, Universitat Politècnica de Catalunya, 2023. https://upcommons.upc.edu/handle/2117/393713 (accessed 2024-05-19).